2. Fundamental Background

2.1. Gold and gold nanoparticles

An overview

The element gold (Latin, *aurum*, Au) was discovered in approximately the 6th century B.C. in free elemental form as nuggets or grains in rocks and has been used for coinage and jewelry since that time.[43]
Up to the 17th century, early chemists (alchemists) such as Paracelsus believed that all materials were a mixture of mercury, sulfur and salts. They thought that by altering the proportions of these base substances and by using the mystic *Philosopher's stone* they could transform them into a noble metal such as gold.[44] However, proof of this hypothesis has never been shown.

Most of the Earth's gold is found at its core and is extracted by screening river sand or with the reduction of rocks. According to the World Gold Council, less than 174,000 tons of gold have been mined in human history.[45]
Currently, gold is widely used in medicine and electronics due to its high malleability, ductility, resistance to corrosion, inertness and conductivity.[46;47]

Gold is a group 11 chemical transition element with the atomic number 79. In bulk, it is solid, dense, extremely soft and ductile under standard conditions. Gold is one of the least reactive chemical elements and it is resistant to oxide formation. It can only be dissolved in aqua regia or in alkaline solutions of cyanide and mercury. Gold appears nearly solely in its elementary form instead of in a compound. Further characteristics will be summarized in **Table SI 1**.[48-50]

Gold features a face-centered cubic crystal structure (fcc, ABCABC). In this type of packing, the atoms of the second layer B are seated in the depressions between the atoms of the first layer A, while the third layer C is placed in octahedral voids[51] (**Figure 2.1a**). Thus, each metal atom is ultimately surrounded by 12 equidistant neighbors and 4 potential adsorption positions on the (111) surface can be defined. It can be situated on top of an atom in the A layer (atop), on top of an atom in the B layer (hcp), on top of an atom in the C layer (fcc) and between two atoms in the A layer (bridge)[51] (**Figure 2.1a**). Adsorption that falls between these positions is also possible, however it is unlikely. The adsorption energies for the four positions was calculated for the methanethiol-gold(111) system and an energy minimum was determined for the fcc position,

A. Barchanski, *Laser-Generated Functional Nanoparticle Bioconjugates*,
DOI 10.1007/978-3-658-13515-7_2

characterizing it as optimal.[52] The distance between two Au atoms is 288.4 pm and each atom has six shells of electrons yielding the electron configuration: [Xe] $4f^{14}5d^{10}6s^{1}$ (**Figure 2.1b**).

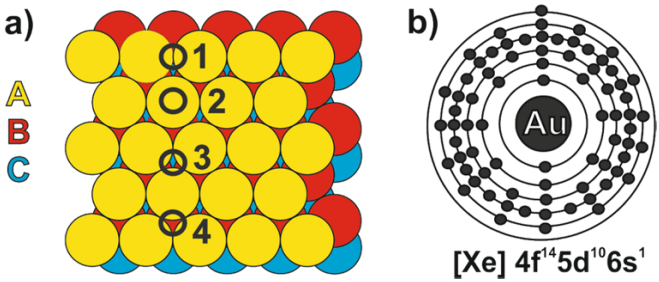

Figure 2.1.Fundamental configuration of gold. a) The face-centered cubic crystal structure (fcc) of gold with three atom layers (**A** = yellow, **B** = red, **C** = blue) and four potential adsorption positions (**1** = bridge, **2** = atop, **3** = fcc and **4** = hcp). **b)** The electron configuration [Xe] $4f^{14}5d^{10}6s^{1}$ of a gold atom (Au) with electrons (dots) positioned on six atom shells.

The dominant oxidation states for organogold compounds are:

- **+I** featuring the coordination number 2, a linear molecular geometry, diamagnetic properties and 14 electron species [d^{10} ions] and
- **+III** with coordination number 4, a square-planar molecular geometry, diamagnetic properties, toxic behavior and 16 electron species [d^{8} ions].[53]

Although gold is inert in bulk form, it features complex ligand chemistry on the nanometer-scale. For instance, an oxidative addition of the S-S bond to a gold surface is enabled by the mechanism as summarized in **eq 2.1**.

$$RS\text{-}SR + 2\ Au_{(s)} \rightarrow 2\ RS\text{-}Au_{(s)}$$

eq 2.1

The binding energy of the RS-SR bond is ~ 65 kcal mol^{-1}.[54]

Whereas, the mechanism for an oxidative addition of the S-H bond to the gold surface, followed by a reductive elimination of the hydrogen is shown in **eq 2.2**.

$$R\text{-}SH + 2\ Au_{(s)} \rightarrow 2\ RS\text{-}Au_{(s)} + H_2$$

eq 2.2

The binding energy of RS-H bond is ~ 86 kcal mol^{-1}.[54]

The released hydrogen could either adsorb on the gold surface or desorb as molecular hydrogen (solubility 1.6 mg L^{-1} in water).[55]

The time it takes to form *full* monolayers has been reported to vary from seconds[56] to minutes[57], up to several hours[58] and sometimes days[59] and both, thiols and disulfides were found to adsorb at the same rate, limited mainly by mass transport.
Even though colloidal gold has been used for centuries e.g. to manufacture the famous Lycurgus Cup (5th century) and later as *Purple of Cassius* in stained church glass (17th century), the first systematic study of its synthesis and characterization was performed in 1857 by Michael Faraday. Faraday discovered that the optical properties of gold submicrometer-sized particles were different from those of the bulk metal[60] and he related the variety of fluid colorations to the particle sizes.[2;60]
However, details on gold nanoparticles' (AuNPs) optical characteristics were declared later by researchers such as Richard Adolf Zsigmondy or Gustav Mie and will be summarized in **Chapter 2.2.**

2.2. Optical aspects of gold nanoparticles and their imaging

Shedding light on cellular processes

A flexible and adjustable size as well as tunable shapes and conformations may be provided for gold nanoparticles, depending on synthesis strategies, the surrounding medium and particle density. These physicochemical differences result in distinct changes in the optical properties, rendering the particles differentiable with microscopy techniques[61;62] such as transmission electron microscopy and by the colloid coloration[63;64] (**Figure 2.2a**).

The unique optical properties of gold nanoparticles are mainly caused by collective oscillations (*localized surface plasmons*, LSP) of conduction band electrons upon excitation with an alternating, electric field of incident electromagnetic radiation.[65;61;66] The field induces a polarization/displacement of the surface electrons relative to the nuclei which develop a restoring force due to the Coulomb attraction between the electrons and the nuclei (**Figure 2.2b**).[32;67]

The electromagnetic radiation is scattered by particle sizes that are similar to or larger than the wavelength of incident light. This scattering is predominantly explained with the Mie solution to Maxwell's equations.[68] In this context, the relationship of extinction, absorption and scattering is given in **eq 2.3**, for the distinct wavelength, particle radius and shape, particle refractive index and refractive index of the medium.

[2] '[…] known phenomena seemed to indicate that a mere variation in the size of [gold] particles gave rise to a variety of resultant colors.'

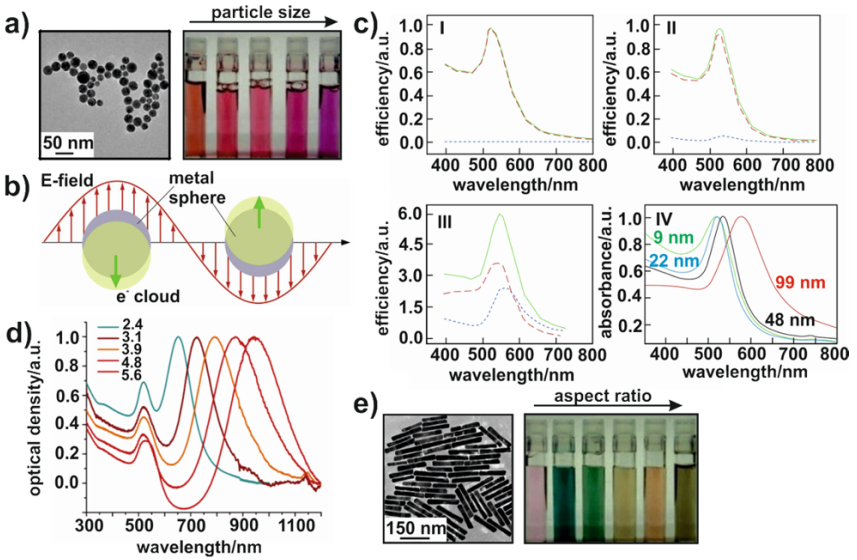

Figure 2.2. Size-dependent and shape-dependent optical properties of AuNPs. a) Left panel: Transmission electron micrograph of gold nanoparticles. Reprinted with permission from Besner et al., copyright 2007 by Springer Science+Business Media.[69] **Right panel:** Photography of gold nanoparticle colloids with increasing particle size. Adapted with permission from Mody et al., copyright 2010 by the Journal of Pharmacy and Bioallied Sciences.[63;64] **b)** Schematic representation of movements in the electron cloud in an electric field that are responsible for the surface plasmon resonance effect of AuNPs. Reprinted with permission from Kelly et al., copyright 2003 by the American Chemical Society.[32] **c)** The extinction of AuNPs (green solid line) is exclusively represented by the absorption cross section (red dashed line) of particles smaller than 20 nm (**I**). With increasing size, a growing component of scattering (blue dotted line) appears as shown for 40 nm (**II**) and 80 nm (**III**) particles. Adapted with permission from Jain et al., copyright 2006 by the American Chemical Society.[70]] In addition, the LSPR band broadens and shifts to longer wavelengths with nanoparticle size increase (**IV**) from 9 to 99 nm. Adapted with permission from Link et al., copyright 1999 by the American Chemical Society.[71] **d)** The LSPR band of elongated AuNPs (gold nanorods) splits into two bands and is presented for different aspect ratios from 2.4 to 5.6. Adapted with permission from Huang et al., copyright 2006 by the American Chemical Society.[72] **e) Left panel:** Transmission electron micrograph of gold nanorods. Reprinted with permission from Vigderman et al., copyright 2013 by the American Chemical Society.[73] **Right panel:** Photography of gold nanorod colloids with increasing aspect ratio. Adapted with permission from Mody et al., copyright 2010 by the Journal of Pharmacy and Bioallied Sciences.[63;64]

$$c_{ext} = c_{abs} + c_{sca}$$

eq 2.3

C_{ext} = extinction cross section, C_{abs} = absorption cross section, C_{sca} = scattering cross section.

Mie scattering is not strongly wavelength-dependent, but the particle size dependence may be illustrated in **Figure 2.2c**. While for small particles of 20 nm in diameter the extinction is exclusively represented by the absorption cross section of the particles (**I**), the Mie scat-

tering contribution starts with particles of 40 nm sizes (**II**) and significantly adds to the extinction of 80 nm AuNPs (**III**).
Conversely, there is another scattering type called *Rayleigh scattering*, which explains the elastic scattering for nanoparticles of much smaller size than the wavelength of incident light. The Rayleigh scattering intensity is proportionate to the 6th power of the particle's diameter and is strongly related to wavelengths in the UV region (230–320 nm).

The LSP can be excited in the UV-vis spectral range and the excitation of LSP resonances (LSPR) leads to an enormous increase in the absorption and scattering cross sections,[74] which are accessible to various imaging strategies as discussed later in this thesis.
Due to the LSPR, AuNPs have an extinction maximum in the green spectral region around 520 nm and the colloid features an intense red coloration. Modifications in the size or shape of AuNPs result in a shift and/or broadening of the LSPR band and in a change of the colloidal color (**Figure 2.2a**, **Figure 2.2d–e**). Therefore, increased scattering and a further red-shifted absorption maximum are mainly related to e.g. increasing particle size, deformation or agglomeration.[71]
Furthermore, for an elongated particle (nanorod) the surface plasmon band splits into two bands (**Figure 2.2d**).[72] The band that absorbs at short wavelengths characterizes the oscillation of the electrons perpendicular to the long rod axis and is referred to as transverse plasmon absorption. The other band that absorbs at higher wavelengths in the near-infrared (NIR) region is defined as longitudinal surface plasmon absorption and is caused by the oscillation of free electrons along the long rod axis.

In addition, the LSPR wavelength is very sensitive to changes in the dielectric properties of the surrounding medium as shown in the framework of the *Drude model* (**eq 2.4–eq 2.6**).[70;75]

$$\lambda_{SPR\,max}{}^2 = \lambda_p{}^2(\epsilon_\infty + 2\epsilon_m)$$

eq 2.4

$$\lambda_p{}^2 = \frac{2\pi\, c^2}{w_p{}^2}$$

eq 2.5

$$w_p{}^2 = \frac{N\, e^2}{m_e\, \epsilon_0}$$

eq 2.6

$\lambda_{SPR\ max}$ = wavelength of the surface plasmon resonance peak of gold nanoparticles, λ_p = bulk plasmon resonance wavelength of gold, ϵ_∞ = high-frequency dielectric constant of gold due to interband and core transitions, ϵ_m = dielectric constant of the surrounding medium, c = speed of light in vacuum, w_p = bulk plasma frequency, N = density of free electrons in the nanoparticle, m_e = effective mass of an electron, ϵ_0 = permittivity in vacuum.

In this context, media with high refractive indices couple stronger with the surface plasmon electrons and the required energy to excite the collective oscillation is reduced. Thus, the LSPR absorbance shifts to lower energy, which correlates with longer wavelengths. By this means, molecules that increase the refractive index near the nanoparticle surface by adsorption will also induce an LSPR shift, enabling sensing applications.[76]

The interband absorption of gold is found at 380 nm and correlates with the atomic concentration of colloidal gold according to results from Muto et al.[77] However, the scattering of aggregates, agglomerates and the couplings of primary particles and nanoparticles with a large diameter is found in the NIR region (**Figure 2.2c IV**, high offset for 90 nm particles at 800 nm wavelength).

Based on optical characteristics of AuNPs, such as a high quantum yield, good signal to noise ratio and the disability of bleaching[71;78;61;79] with the described tunable spectroscopic characteristics, a ground-breaking study was conducted to replace conventional fluorescent dyes by the AuNPs, especially in relation to longer time-scale observations in living specimen.[65;80;61] Various imaging strategies were developed and adopted for this intent.
The classical standard for the visual characterization and quantification of gold nanoparticles in dispersion and in their spatial distribution in fixed samples is the transmission electron microscopy (TEM).[81] The very high contrast of gold renders these particles easily distinguishable within cellular structures. The method can only be applied on very thin preparation sections and detailed information about size distributions of the particles and their arrangements within intracellular structures can be validated.[82-85] For example, Chithrani et al. imaged and counted single gold nanoparticle spheres of different sizes from 14 to 100 nm in high resolution within endosomal vesicles (**Figure 2.3**).[82]

In addition, Murphy et al. presented differently shaped gold nanostructures with increasing diameter and aspect ratio, that were easily distinguishable from each other on TEM micrographs.[84] However, the detection of lead or osmium artefacts from the fixation protocol cannot be excluded and the investigation of *in vivo* processes is not feasible with this method. Thus, electron microscopic approaches such as TEM or STEM (scanning transmission electron microscopy) provide indispensable basic knowledge about nanoparticle composition and intracellular distribution, but are limited in their application on living biosystems.

Nanoparticles are per definition less than 100 nm in diameter, which is only half the size necessary to meet the refraction limit for light microscopic detection of single particles. However, due to the high quantum yield in absorption and scattering of AuNPs it was demonstrated repeatedly that single particles could be visualized by optical microscopy from 5 nm onwards using the absorption cross section for differential interference con-

trast (DIC) microscopy[86-88] and using the scattering for 40 nm onwards for optical coherence tomography (OCT)[89;90] and reflection based (dark field) microscopy.[76;91;79;92]

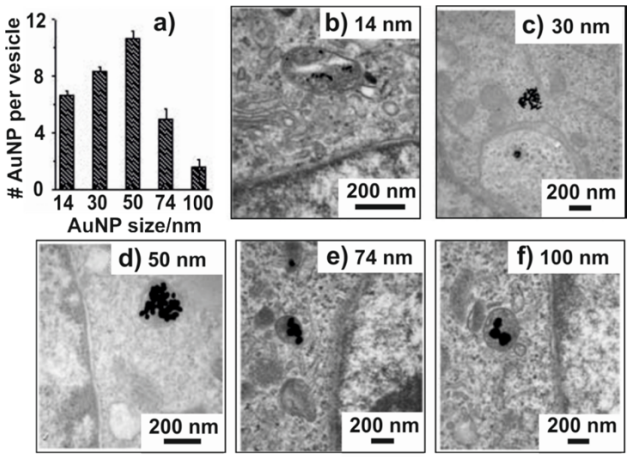

Figure 2.3. Example of AuNP imaging by TEM. Transmission electron microscopy provides information on the number, size and arrangement of particles in organic structures and allows for the quantification of nanoparticles within distinct cell compartments. **a)** Number of counted AuNPs per vesicle as function of particle size. **b)–f)** Transmission electron micrographs illustrating endocytosed AuNPs inside of intracellular vesicles for AuNP diameters of **b)** 14 nm, **c)** 30 nm, **d)** 50 nm, **e)** 74 nm, **f)** 100 nm. Adapted with permission from Chithrani et al., copyright 2006 by the American Chemical Society.[82]

In this context, the differentiation of single or aggregated AuNPs was presented using the LSPR scattering-based confocal laser scanning microscopy (CLSM).[92;93] Klein et al. successfully displayed dispersed single gold nanoparticles from diameters of 60 nm onwards (**Figure 2.4a–b**), while particles of 15 nm diameter could be imaged after aggregation (**Figure 2.4c**).[93]

Since intracellular particle aggregation is common, all size classes were imaged after co-incubation with bovine immortalized endothelial cells (**Figure 2.4d–f**). Thus, a differential imaging of aggregated versus dispersed gold nanoparticles by specific light scattering of aggregates and single particles in different wavelength regions is feasible for imaging throughout the visible spectrum.

As explained earlier, the spectral properties of imaged nanoparticles are indicative of the current status of the nanoparticle dispersion and could provide information on size, shape and functionalization of gold nanoparticle constructs *in vitro* and even *in vivo*.

In this context, the LSPR scattering-based, vibrational, surface-enhanced Raman spectroscopy (SERS) may be used to gain information about the chemical composition of a sample in the close vicinity of AuNPs. For instance, Sezgin et al. applied SERS for prob-

ing the cellular environment of AuNPs after their introduction into living cells and differentiated their accumulation areas based on molecular level differences.[94]

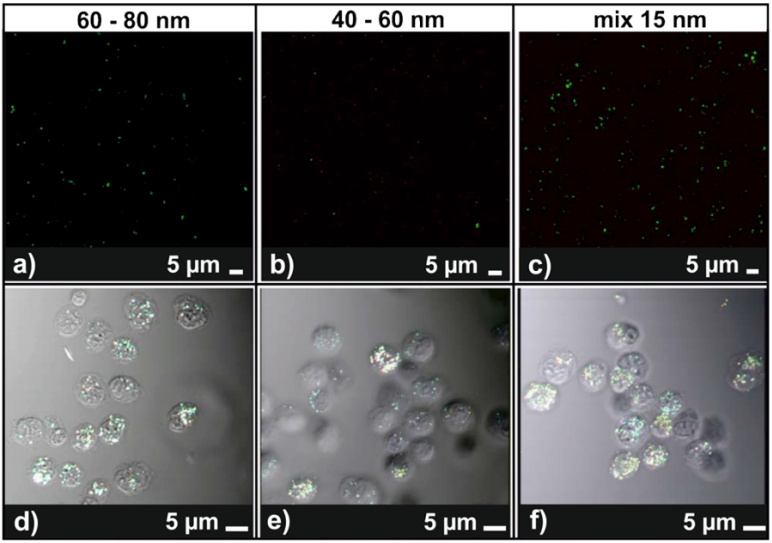

Figure 2.4. Example of AuNP imaging by CLSM. a)–c) Confocal imaging of the LSPR scattering (green dots) from differently sized AuNPs at equal number concentrations in dispersion. **d)–f)** The LSPR scattering from differently sized AuNPs after 48 h co-incubation with bovine endothelial cells. Only dispersions of 60–80 nm-sized particles allowed visualization of single particles in dispersion. However, the aggregation and containment of particles within cells enhanced the scattering cross section to visualize also the smaller particles. Adapted with permission from Klein et al., copyright 2010 by the Society of Photo Optical Instrumentation Engineers.[93]

Addressing *in vivo* imaging, a very unique property of a noble metal such as gold is the photothermal effect[95] that allows the independent localization[96] and treatment of gold nanoparticles after excitation with light independently from other, non-metal particles in the same field. Werner et al. and Lasne et al. demonstrated the tracking of 5 nm gold beads in living cells using this technique.[97;98] Both reports emphasized the extremely low background noise that also exists in scattering environments such as cells and tissues. Furthermore, the photoacoustic detection of AuNPs by shock wave generation upon pulsed particle heating was also reported.[99;100]

It can be summarized, that gold nanoparticles feature unique optical characteristics that are mainly due to the localized surface plasmons. The resulting flexibility of the spectral properties that correspond to the particle's size, shape and surface functionalization enables the clear identification of the specific state of AuNPs and highlights them as suitable material for biomarker research.

Various imaging techniques were adopted in order to detect AuNPs within biological samples and living specimens. A size-selective imaging of small gold nanoparticles after cellular penetration is applicable using light and electron microscopic methods. Thereby, it is feasible to visualize particle aggregation and their quantitative accumulation selectively by employing scattering-based approaches such as confocal laser scanning microscopy. Other methods can also be used, such as optical coherence tomography or the photothermal and photoacoustic detection that enable even the *in vivo* visualization of AuNPs.

2.3. Toxicological aspects of gold nanoparticles

The dose makes the poison

The toxicity of AuNPs is a very complex topic because the level of toxicity is highly dependent on the size, concentration, shape and surface chemistry of the particles as well as on the experimental design involving animal or cell culture models and the methods used to characterize particle localization and distribution.[101] Standardized methods for toxicological assays with nanoparticles are not widely applied, although the Organization for Economic Co-operation and Development (OECD) has recommended general guidelines in 2012.[102] Thus, it is not surprising that results are very different for each case and vary significantly. However, by reviewing a variety of toxicological studies, an estimation of the toxicity mechanisms and thresholds can be determined.

In contrast to the bulk material, nanoscaled particles feature a higher reactivity and toxicity, which is mainly derived from their high mass-specific surface area per mass ratio with surface-specific dose-response.[103;104] The mechanisms of cellular damage caused by nanoparticles are explained by the interactions at the nano-bio interface,[105-108] resulting mainly in the affection of DNA[109;110] and the production of reactive oxygen species[104] (ROS). This can cause inflammation or even malignant transformation of somatic cells. For instance, Liu et al. described an interaction of 1.4 nm sized AuNPs with B-form DNA while causing its transition to A-form DNA.[109] However, ROS formation is generally found for nanoparticles featuring a band gap structure, e.g. semiconductor metal nanoparticles.[111]

The parameters that affect nano-bio interactions are the size, shape, charge and functionalization of AuNPs. This variety makes it difficult to find a satisfactory comparison of toxicity studies. However, a selective overview of recent publications and their AuNP parameter dependence is shown in **Table SI 12**, while for deeper insight, the readers are referred to other review articles.[104;84;112;34;101;113-115]

Most of the available literature tends to cover the *in vitro* toxicity of AuNPs (**Table SI 12**) due to the experimental freedom that allows for a much broader dosing and testing range compared to *in vivo* studies, whose numbers are usually kept low for ethical reasons. The toxicity discovered in those *in vitro* studies ranged from negligible and regardless of the used particle type[116-118] to intermediate[119-123] and even severe.[124-127] However, various cell lines were applied for the studies which may respond completely different on the same nanoparticle exposure. It was further demonstrated, that primary cells differ in sensitivity towards nanoparticle-derived toxicity than the corresponding cancer and immortalized cell lines.[128;129]

A size-dependent cytotoxicity of AuNPs was found by Pan et al., when they analyzed the size ranges from 0.8 to 15 nm.[124] They found that AuNPs with sizes from 1 to 2 nm raised significant toxic effects in four cell types, while even a minor decrease in size (from 1.8 to 1.4 nm) may increase the toxic effect by 4-6 factors.[124] 15 nm-sized particles provided comparably no cytotoxic effect. Further, Pan et al. identified that 1.2 nm-sized AuNPs mainly induced cell death by apoptosis while 1.4 nm-sized particles were responsible for cell death by necrosis (**Figure 2.5a**).[124] However, Pan et al. applied a high particle number dose and surface area, which is critical according to a study on airborne nanoparticles from Oberdorster et al., who demonstrated that the main parameter for adverse effects in biological systems is the particle surface area.[104]

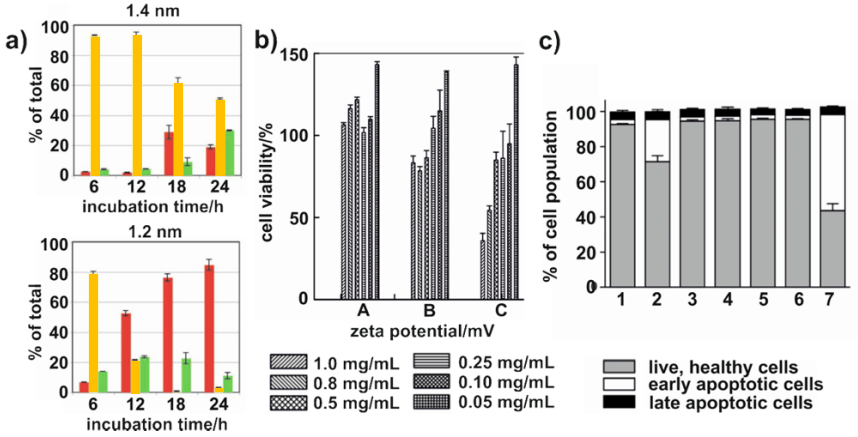

Figure 2.5. **Examples on the *in vitro* toxicity of AuNPs and AuNP bioconjugates. a)** Influence of particle size on the *in vitro* toxicity of AuNPs. Red bars = necrotic cells, yellow bars = live cells, green bars = apoptotic cells. Adapted with permission from Pan et al., copyright 2007 by John Wiley & Sons Inc.[124] **b)** Influence of particle charge on the *in vitro* toxicity of AuNPs. **A** = +20 mV, **B** = +30 mV, C = +40 mV. Adapted with permission from Ding et al., copyright 2010 by the American Chemical Society.[127] **c)** Influence of particle surface modification on the *in vitro* toxicity of AuNPs. **1** = untreated control, **2** = citrate, **3** = BSA, **4** = ssDNA, **5** = dsRNA, **6** = Doxorubicin. Adapted with permission from Massich et al., copyright 2010 by the American Chemical Society.[121]

The impact of AuNP charge was analyzed at the particle-liquid-interface by Ding et al., who discovered a distinct correlation between cytotoxicity and an increase in positive surface charge[127] (**Figure 2.5b**). This result was further confirmed in a study by Goodman et al., in which they compared 2 nm-sized cationic and anionic AuNPs.[130] While the cationic AuNPs provoked pronounced cell lysis, the anionic AuNPs featured a low cytotoxicity which was most likely due to the weak electrostatic interactions with the cell membrane.[130] In addition, Bartneck et al. found in a more detailed study that carboxyl groups on the particle surface induced the expression of mRNAs which encode pro-inflammatory proteins, while amino groups on the particle surface induced mRNAs which encode anti-inflammatory proteins.[131]

During chemical synthesis, AuNPs are often stabilized by sodium citrate molecules, which change the surface conditions of the nanoparticles. Such citrate-stabilized AuNPs were found to induce significant changes in the gene expression profile of HeLa cells[121] (**Figure 2.5c**). However, when the stabilizing agents were disclaimed, Salmaso et al. did not observe any toxic effect up to a concentration of 0.74 nM gold,[117] while Taylor et al. noticed an effect, but only at five times higher AuNP concentrations of ~ 5 nM for ultrapure, laser-generated AuNPs.[122] Thus, the cytotoxic impact of nanoparticle surface ligands should always be considered and systematically studied in comparison to ligand-free reference nanoparticles (e.g. AuNPs fabricated by pulsed laser ablation in pure *MilliQ*).

Acknowledging Paracelsus' doctrine,[3];[132] an AuNP threshold concentration/dose for the initiation of toxic effects must exist. Unfortunately the AuNP concentration in all studies (**Table SI 12**) varied widely and different sizes, shapes and charges were adopted. Thus to date, no comparability can be given for a universal threshold determination.
Khlebstov and Dykman proposed a general limiting dose of ~ 10^{12} particles per mL for AuNPs within the size-range from 3 to 100 nm.[101] However, mass dose, number dose and surface dose have to be differentiated in this context (**Figure 2.6a**).
As illustrated on **Figure 2.6a 1** the same particle mass concentrations can be obtained by using many small or fewer large particles with completely differing surface area.[115] Thus, studying the toxicological effect of nanoparticles with different sizes at equal mass doses it is impossible to clarify which variable (particle size, particle number, particle concentration or particle surface area) is the determining factor (**Figure 2.6b**).[115] Moreover, Taylor et al. recently declared that 'drastic effects caused by very high *unrealistic* exposure values may be over-interpreted, while subtle effects due to low-dose *realistic* exposures may be overlooked'.[115]

[3] 'Dosis facit venenum' = it is the dose that makes the poison.

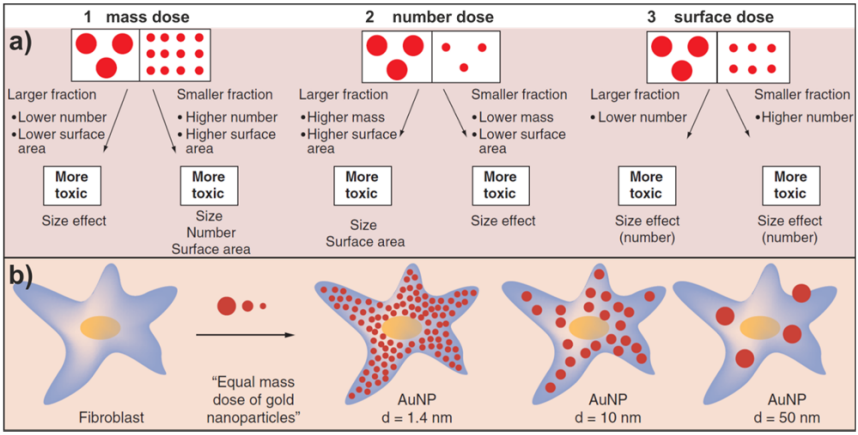

Figure 2.6. Schematic illustration of nanoparticle dose expression. a) Comparison of two nanoparticle size classes (larger fraction = left box, smaller fraction = right box) that are equivalent to the same nanoparticle mass dose (**1**), nanoparticle number dose (**2**) and nanoparticle surface dose (**3**), showing that most information is accessible from the surface area of the dose. **b)** The degree of surface coverage with differently sized nanoparticles of the same nanoparticle mass dose is presented on the example of a fibroblast. Reprinted with permission from Taylor et al., copyright 2014 by Taylor et al., licensee Beilstein-Institute.[115]

It is important to consider further, that the applied particle dose in the cell culture medium is rarely identical with the delivered dose that the cells come into contact with and the cellular dose that is internalized by the cells.[115] In the style of the toxicological testing of airborne particles, Oberdorster et al. recommended to express the applied dosage as particle surface area concentration (e.g. cm^2 of nanoparticles per mL).[104] However, as the toxicological effect is highly dependent on the cell number, an expression of dose per cell density, organ mass or organ surface area (e.g. cm^2 nanoparticles per cell number or cm^2 nanoparticles per g of biomass) is highly recommended by the OECD.[102]

The ability of AuNPs to effectively cross the blood-testis-barrier after intravenous injection was recently documented by Balasubramanian et al.[133] Therefore, concerning biological reproduction, the toxic effects of gold nanoparticles on gametes should be considered, because this might result in impaired fertility and/or congenital defects of the offspring. Unfortunately, only a few studies have focused on this topic thus far (**Table SI 12**).[134] For instance Wiwanitkit et al. discussed the morphological defects and motility decrease of human spermatozoa after treatment with citrate-stabilized AuNPs.[135] However, no information on the adopted particle dose was provided. Tiedemann et al. determined no toxic effects on boar spermatozoa after incubation with 10 $\mu g\ mL^{-1}$ AuNPs,[136] while Taylor et al. and Moretti et al. reported membrane-attachment and a dose-dependent decrease of bovine/human spermatozoa motility after incubation with

50–500 µM AuNPs[137;138] (**Figure 2.7a**). However, Tiedemann et al. adopted serum protein-stabilized, non-aggregated particles, while aggregated AuNPs were applied in the other studies. Gold aggregates are subject of fast sedimentation in cell culture and feature a different cellular interaction and uptake behavior than non-aggregated nanoparticles (see **Chapter 2.4.**).

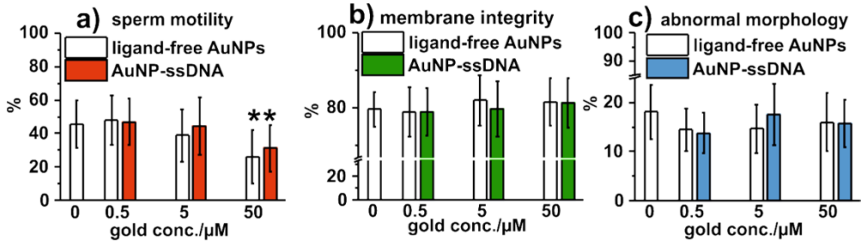

Figure 2.7. Examples on the reprotoxicity of AuNPs and AuNP bioconjugates. The effects of ligand-free AuNPs (white bars) and AuNP-ssDNA bioconjugates (colored bars, 0.5–50 µM concentration) on bovine spermatozoa characteristics. **a)** Effect on sperm motility. * ANOVA, $p \leq 0.5$. **b)** Effect on membrane integrity. **c)** Effect on sperm morphology. Results are presented in comparison to an untreated negative control (0 µM). Based on data from Taylor et al., copyright 2014 by Taylor & Francis.[137]

The concentration range from 50–500 µM AuNP significantly exceeds the number of nanoparticles that are required for scientific or medical applications. Furthermore, Taylor et al. found that there was no effect on membrane integrity and spermatozoa morphology after AuNP incubation (**Figure 2.7b–c**).[137] However, Zakhidov et al. found that very small AuNPs with diameter of 2.5 nm disrupted nuclear chromatin decondensation in mouse spermatozoa.[139]

The penetration of AuNPs into ovaries or follicles has not been studied to date, but Tiedemann et al. found no toxic effects on oocyte maturation after treating the cumulus-oocyte complex with AuNPs up to a concentration of 30 µg mL^{-1}.[136]

When looking at the developmental toxicity and fetal impairment that can occur with AuNPs, two separate studies with rodent models analyzed and confirmed their transfer across the placental membrane (**Table SI 13**).[140;141] Interestingly, two other studies could not find any particle transfer.[142;143] In addition, in an *ex vivo* model by Myllynen et al. no placental AuNP transfer was detected, which illustrates the difficulty to determine whether or not this transfer actually occurred.[144]
Further developmental toxicity of gold nanoparticles was analyzed in zebrafish,[145;146] chicken[147;148] and murine[149] embryos. Although the presence of AuNPs inside the embryos was proven, [145;146;149] no toxic effects were determined in the studies. However, a recent publication on zebrafish detected an embryotoxic effect of gold clusters after applying a number dose of 10^{14} NP per embryo.[150] Furthermore, the toxicity depended

on particle size and ligand chemistry and AuNPs with covalently bound ligands were determined to be less toxic than AuNPs with electrostatically bound ligands.[150]

Examining the *in vivo* studies of AuNP toxicity on developed (adult) animals (**Table SI 12**), a size-dependent effect on BALB/C mice was determined by Chen et al. In their study they investigated AuNPs with diameters from 3 to 100 nm and found a significant lethality for mice treated with AuNPs with diameters between 8 and 37 nm, while other sizes did not induce any effect.[151] Other studies described various effects of AuNPs, covering expressed changes of the inner organs[96] and abnormal up and down regulation of genes[133] in rats, induced inflammation and apoptosis in mice[152] and induced oxidative stress in mytilus edulis.[153]
Conversely, other studies did not discover any toxic effects of 1.9 to 100 nm-sized AuNPs in mice and pigs although a dose-dependent accumulation in various organs was determined.[154-158]
In 1997, a clinical study was performed by Abraham et al. on 10 rheumatoid arthritis (RA)-affected humans, using 20 nm-sized Aurasol® AuNPs at a daily oral administration of 30 mg, over a period of up to 5 months.[159] Interestingly, they not only found the administration to be non-toxic, but determined that various RA-relevant factors were significantly suppressed when the subjects reported an improvement in joint pain, swelling and mobility.[159] However, the production of Aurasol® has now been discontinued without any information about the reasons.
In general, the *in vivo* studies indicate that low doses of AuNPs ($< 400\ \mu g\ kg^{-1}$) do not appear to cause appreciable toxicity, [158;160] although at higher concentrations, severe sickness, shortened survival time and liver inflammation were observed.[151;152]

In summary, the toxicological aspects of gold nanoparticles remain up for debate because of the variety of parameters that influence the particles' toxic behavior and the incomparability among toxicological studies. Especially the expression of *particle dose* is a crucial aspect for the evaluation and comparability of toxicological studies. Up to now there are no general regulations or standardized methods for toxicology assays with colloidal nanoparticles. For instance the same particle mass concentration dose may be obtained by using many small or fewer large particles with completely differing surface area. However, the indication of a *nanosurface per bio* dose additionally to the common mass concentration dose in the format of 'surface area dose of nanoparticles referenced to the cell number or organ mass' may overcome this issue in the future.[115]

2.4. Gold nanoparticle-membrane interactions

How to cross barriers and where to go

Controlled nutrient uptake and the disposal of contaminants are essential for cells to sustain metabolism. To provide differentiation and maintain controllability of this survival process, evolution has naturally developed several uptake and transport mechanisms.[161-164] Ions and small molecules usually migrate along concentration gradients and may enter cells via an unspecific diffusion process. Conversely, macromolecules are mainly internalized energy-dependent by endocytosis after a specific interaction occurs with their texture and membrane-associated surface receptors.
In this context, it is obvious that the cellular uptake and the uptake mechanism of gold nanoparticles is not only affected by their size and shape but also by their steric (e.g. nature/amount of conjugated ligand) and electrochemical (e.g. surface charge) properties. They may also be dependent on the studied cell line because each cell line exhibits different phenotypes and receptor expression levels (**Figure 2.8a**).

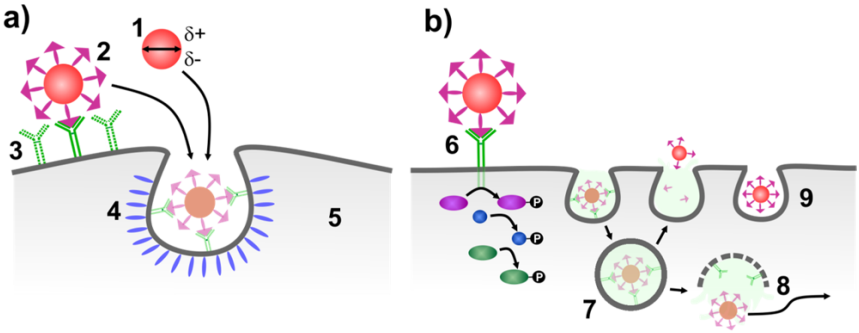

Figure 2.8. Cellular uptake and intracellular fate of AuNPs. a) Factors that can influence the interactions between nanoparticles and cells at the nano-bio interface (**1** = size, shape, charge; **2** = ligand density; **3** = receptor expression level; **4** = internalization mechanism; **5** = cell properties such as phenotype and location). **b)** Potential interaction of nanoparticle bioconjugates with cells (**6** = antibody-coated NPs bind specifically to membrane receptors and induce a signaling cascade without entering the cell; **7** = endocytosis/exocytosis of nanoparticle bioconjugates without leaving the vesicle; **8** = endocytosed nanoparticle bioconjugates escape from the vesicle and interact with organelles such as the nucleus, mitochondria or actin filaments; **9** = unspecific internalization of nanoparticle bioconjugates into cells without membrane receptor interaction). Based on a figure from Albanese et al., copyright 2012 by Annual Reviews.[112]

In addition to the possibilities of unspecific diffusion, NP-receptor interaction and specific, receptor-mediated uptake, the intracellular fate of nanoparticles is also of great importance for biomedical application, especially if distinct organelles need to be targeted e.g. the nucleus for gene silencing issues or lysosomes for treatment of the lysosomal

storage disease. Thus, specific ligands may be required to induce intracellular signaling cascades, to enable the escape of endocytotic vesicles and to reach the area of interest (**Figure 2.8b**).

A number of studies are currently being done on the influence of the intrinsic properties or gold nanoparticles and their functionalization for cellular penetration. A selection of these studies has been summarized in **Table SI 13**. Readers are also encouraged to examine other review articles to gain a deeper insight into this subject.[112;34;165;166;101;167]

Several studies have demonstrated that the cellular effects of AuNPs depend on their size, shape and surface charge (**Table SI 13**) [82;168-171].

With regard to size, the cell membrane wrapping time of nanoparticles was investigated by Gao et al.[172] In their hypothesis, the cellular uptake was considered to be a result of competition between the thermodynamic driving force for wrapping (amount of free energy to drive nanoparticles inside cells) and the receptor diffusion kinetics (kinetics of recruitment of receptors to the binding site). These two factors determine how rapidly and how many nanoparticles are taken up by the cell. Gao et al. proposed that the docking of a nanoparticle with a size that is smaller than 50 nm would not produce enough free energy to be completely wrapped and that the fastest wrapping time would occur for nanoparticles that were 55 nm in diameter.[172] Thus, to facilitate the efficient cellular internalization of small nanoparticles, they must be clustered. However, for nanoparticles that are larger than 60 nm, the receptor diffusion kinetics and thereby the wrapping time is slower, which leads to a fewer number of particles being internalized.[172] According to this suggestion, Chithrani et al. investigated the uptake of spherical gold nanoparticles that ranged in diameter from 10 to 100 nm. They determined that 50 nm primary nanoparticles were able to enter the cells with high efficiency (**Figure 2.9a**), while the 14 nm species required approximately 6 nanoparticles to cluster together before uptake occurred.[168]

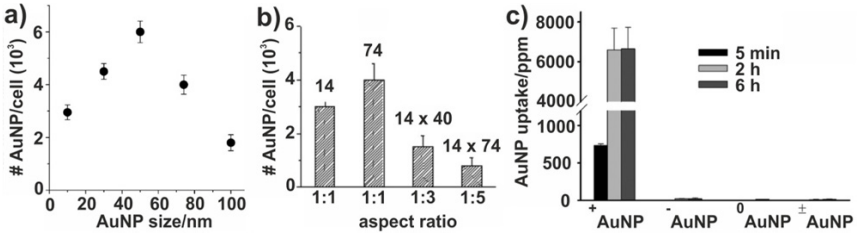

Figure 2.9. Examples on the cellular uptake of AuNPs. a) Number of internalized AuNPs per cell as function of AuNP size. Reprinted with permission from Chithrani et al., copyright 2007 by the American Chemical Society.[168] **b)** Number of internalized AuNPs per cell as function of AuNP size and shape. Aspect ratio 1:1 = spheres, aspect ratio 1:3 & 1:5 = rods. Reprinted with permission from Chithrani et al., copyright 2006 by the American Chemical Society.[82] **c)** Cell uptake of AuNPs as function of particle surface charge. Reprinted with permission from Arvizo et al., copyright 2010 by the American Chemical Society.[171]

In line with Gao's suggestion, they confirmed that particles smaller and larger than 50 nm were internalized to a lesser extent (**Figure 2.9a**).[168] These results were further confirmed by other studies that analyzed size-dependent cell internalization of AuNPs.[169;173;174]
However, concerning the intracellular fate and nuclear internalization, predominantly small AuNPs with diameters < 10 nm were detected inside the cell core, which indicates a size limitation for translocation through the tight nuclear pores.[175-179]

Various studies concerning the influence of AuNP shape on cellular uptake were also performed and are summarized in **Table SI 13**.[168;170;85] Thereby, the uptake of spherical 14 nm and 74 nm gold nanoparticles was determined by Chithrani et al. to be approximately 3 orders of magnitude higher when compared to rod-shaped gold particles with aspect ratios of 1:3 and 1:5[82] (**Figure 2.9b**). They considered this effect to be potentially curvature-dependent, because the contact area of rod-shaped particles is larger than for spherical NPs when the longitudinal axis of the rods interacts with the cell membrane receptors.[82] On the contrary, Bartneck et al. found that there was an up to 230 times more efficient uptake of gold nanorods into macrophages than of gold spheres with the same diameter.[131] However, considering the function of macrophages as a non-specific immune defense to engulf and ingest pathogens, Bartneck et al. speculated that the morphological similarity of nanorods to protein capsules of virus particles may support their increased uptake.[131]

With regard to surface charge, several studies concluded that cells in serum-free media internalize positively charged gold nanoparticles with higher efficiency than negatively charged or uncharged particles (**Table SI 13**, **Figure 2.9c**).[180;171;181-183] This is most likely due to the high affinity of positively charged species to a negatively charged cellular membrane.[184] However, Arvizo et al. found this effect to be based on the depolarization of plasma membrane potential.[171] Since baseline membrane potential was determined to range between -75 and -55 mV, only positively charged gold nanoparticles were determined to induce this depolarization.[171] The depolarization effect might cause the loss of rigidity and initiate morphological changes of the cell.[185] Thus, to maintain the original charge distribution, Cho et al. suggested that the plasma membrane must remove the attached gold nanoparticles e.g. by delivering AuNPs in intracellular vesicles (endocytosis),[185;180] or by other mechanisms that deliver AuNPs directly into the cytosol.[117;122] Since positively charged nanoparticles are attached more affine to negatively charged membranes than negatively or neutral charged species, cationic particles will consequently be internalized more easily and efficiently by the cells than anionic, zwitterionic or neutral NPs. In addition, Ding et al. correlated the zeta potential of AuNPs with their transmembrane efficiency and found that those with higher potential were internalized more quickly with enabled nucleus targeting than NPs with lower zeta potential.[127] How-

ever, if surface potential is too high, the particles may destabilize the cell membrane and induce cell damage and cytotoxicity.
A mechanism for the AuNP uptake of negatively charged species was discovered by using serum-containing cell culture media.[82;186] Chithrani et al. found that serum proteins were binding preferential to negatively charged gold nanoparticles and assisting them to enter the cells. By this means, gold nanoparticles that are functionalized with both positively charged and negatively charged ligands may be inserted into cells, if the culture medium is carefully considered.
Moreover, the surface charge of nanoparticles has also been examined in order to potentially determine the intracellular fate of particles. In this regard, Panyam et al. reported that endosomal escape was preferentially observed for cationic nanoparticles compared to anionic ones.[187]

In a similar manner, the surface modification of specific ligands has been reported to provide inefficiently internalized gold nanoparticles with the ability to specifically overcome obstacles such as cellular membranes or vesicles.[123;188-190;175] They were also shown to accumulate at the area of interest. For instance, Verma et al. reported on the highly efficient cellular uptake of gold nanoparticles which were covered with ordered arrangements of hydrophilic and hydrophobic functional groups (**Figure 2.10a**, inset).[189] This specific arrangement facilitated the transport of particles with 4-5 nm in diameter into the cytosol (**Figure 2.10a**) by enhancing the free energy for membrane wrapping, while other ligand distributions on the particle surface resulted in lower uptake efficiencies.

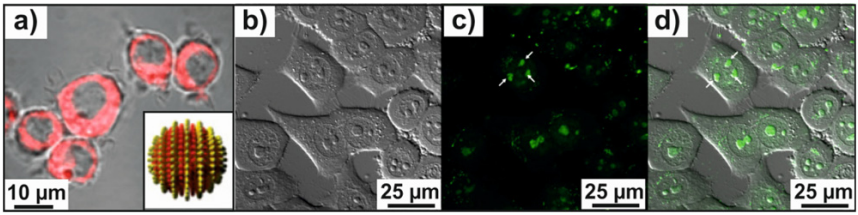

Figure 2.10. Examples on the cellular uptake of AuNP bioconjugates. a) The intracellular distribution (red coloration) of nanoparticles with ordered arrangements of hydrophilic and hydrophobic surface functional groups on confocal image with schematic illustration of ligand shell structure presented in the inset. Adapted with permission from Verma et al., copyright 2008 by the Nature Publishing Group.[189] **b)–d)** confocal images showing **(b)** the DIC, **(c)** the fluorescent image and **(d)** the merged DIC and fluorescence image of HeLa cells treated with AuNP@MPA-PEG-FITC conjugates and the intranuclear accumulation and clustering of nanoparticles (green dots). Reprinted with permission from Gu et al., copyright 2009 by Elsevier.[176]

Specific biological ligands have also been adopted as *Trojan horses* to support the cellular internalization of AuNPs. Besides viral vectors[191] and dendrimers,[192] also peptides that contain protein transduction domains (PTD) have been used in several studies to effi-

ciently transport particles across cell membranes.[193-195] The internalization mechanism of these so-called *cell-penetrating peptides* (CPP) is strongly dependent on the cargo molecule as well as on the adopted peptide concentration.[188;196-198] Both the translocation of AuNPs directly into the cytosol[175;190;83] and their controlled endosomal uptake by endocytosis[196;197;199] have been discussed by CPP support. Tkachenko et al. and Berry et al. reported on the most common CPP termed *TAT* (transactivator of transcription), which was derived from the human immunodeficiency virus type-1 (HIV-1). This TAT was shown to efficiently deliver gold nanoparticles into cells and even the nucleus if the particle size was smaller than the nuclear pore size.[123;200] The nuclear transport was further compared with tiopronin-TAT functionalized gold nanoparticles and a tiopronin-functionalized species without TAT.[175] Numerous tiopronin-functionalized particles were detected in the cytosol, while the tiopronin-Tat conjugates were visualized inside the nucleus. In addition, the functionalization of small-sized gold nanoparticles (< 5 nm) with (poly)ethylene glycol (PEG)[176] or a nucleus translocating signal (NLS) was reported to be highly effective for particle accumulation in the cell core (**Table SI 13**, **Figure 2.10b–d**).[123;83;196;198] However interestingly, Krpetic et al. found that after 24 hours, both the AuNP-CPP and the AuNP-NLS bioconjugates were exocytosed from the cells again.[201]

When looking at the medical application of gold nanoparticles it is important to note that not only their distribution and fate inside a cell, but also their biodistribution in the organism and their clearance from the body must be considered. For this intent, several *in vivo* studies were performed to analyze AuNP accumulation in specific organs of mice, rats and pigs (**Table SI 13**). Most reports describe a significant accumulation of AuNPs in the liver and spleen of the animals, indicating that the nanoparticles most likely bind to plasma antibodies and are subsequently recognized by the phagocyte-rich reticulo-endothelial system (RES).[133;202;143;203;204] In one study, Sadauskas et al. actually described the differentiated particle accumulation in the immune Kupffer cells of the liver,[143] which were in line with observations from Fent et al.[154]
Further accumulation areas of AuNPs within the organism were found in the kidneys and the testis,[133;202] in the lungs,[133;154;156;204] in the heart and the thymus,[202] in the retina[157] and also in the neural tissue after crossing the blood-brain-barrier.[158;204] A size-dependence in the tissue penetration of AuNPs was thereby determined by Sonavane et al.[204] In one study, AuNPs with 15, 50, 100 and 200 nm in diameter were administered intravenously in mice. The 15 nm-sized particles were found to yield the highest amounts in all organs including the blood, liver, lung, spleen, kidney, brain, heart and stomach. In contrast, only a minute presence of 200 nm AuNPs was found in all organs 24 hours after injection.[204] Moreover, Semmler-Behnke et al. found a size-dependent crossing of the air-blood-barrier after intratracheal administration of AuNPs, with small

particles < 2 nm being efficiently transferred, while larger-sized particles (18 nm) were trapped in the lung.[141]

Once they have penetrated into different tissues, NPs can have a long retention time. For example, in the respiratory tract, the mid-life for NPs was found to be approximately 700 days in humans.[104] Moreover, Terentyuk et al. found that smaller AuNPs (15 nm) circulated longer in the organism than for larger-sized ones (50 nm).[96] In this regard, Zhang et al. further determined that 20 nm-sized AuNPs have best blood pool activity and tumor uptake, while 40 and 80 nm-sized AuNPs were cleared readily from the body by uptake in the liver and the spleen.[160]

Because the particle concentration in the organs decreased over time, it appears likely that AuNPs are re-translocated into the bloodstream through lymphatic vessels.[133;204;96] However, a different study presented that AuNPs were efficiently released into the urine after 5 h through filtration in the renal glomeruli.[205] In a more focused study, Zhang et al. detected BSA-conjugated AuNPs that aggregated to 40–80 nm-sized clusters *in vivo* mainly accumulated in liver and spleen, while glutathione-conjugated AuNPs of 5–30 nm cluster size were highly efficiently cleared by the kidneys (**Figure 2.11**).[206]

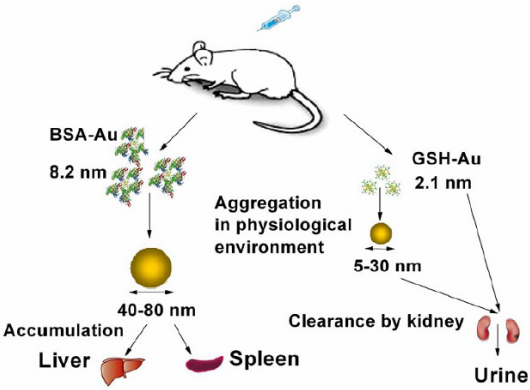

Figure 2.11. Size-dependent accumulation and clearance of AuNP bioconjugates from the organism. Aggregated BSA-AuNPs of 40-80 nm cluster size accumulated in liver and spleen, while GSH-AuNPs of 5–30 nm cluster size were removed from the body by renal clearance. Reprinted with permission from Zhang et al., copyright 2012 by Elsevier.[206]

Similar results were also determined by Zhou et al. who found that after 24 hours, more than 50 % of the 2 nm-sized glutathione-AuNPs that had been administered to mice, was in the urine. This was a 10 to 100 times better clearance than for comparable cyste-

ine-AuNPs.[207] Thus, it can be stated that both the particle size and the attached ligand can influence the biodistribution and the clearance of AuNPs.

In summary, the intrinsic properties of gold nanoparticles, such as particle size, shape and charge as well as their functionalization with penetration agents have a strong influence on their cellular uptake behavior. The intracellular fate and internalization efficiency of particles may be tuned individually by the nanoparticle design, according to the desired uptake mechanism and biomedical indication. Regarding biodistribution, it is assumed that a size- and ligand-dependent biodistribution with tissue accumulation of AuNPs in the liver and spleen is favored, while small particle sizes (< 30 nm or < 10 nm) may be removed from the organism by renal clearance.

2.5. Biological application areas of gold nanoparticles

Golden age of modern diagnostics and therapy

Although gold nanoparticles and gold nanoparticle bioconjugates are monitored for a multitude of novel research concepts, three main application areas in biomedical and reproduction-related research may be defined thus far:
(**I**) Selective targeting [208;2] and sensing [209;4] of molecules or cells, e.g. for detection, imaging and sorting issues.
(**II**) Localized, photothermal cancer therapy by plasmonic heating of malignant tissue.[5]
(**III**) Delivery and switchable release of effector molecules to specific receptors/at the area of interest.[210;6]

Selective targeting and sensing
The targeting, sensing and imaging of molecules by gold nanoparticle bioconjugates relies mainly on their interaction with light. As presented in **Chapter 2.2**, gold colloids display an intense red color due to the LSPR, which may be utilized as a non-photobleaching alternative label to fluorophores. Therefore, particles must be functionalized with recognition moieties (e.g. antibodies) for the specific detection of target molecules (e.g. antigens) according to the lock-and-key principle (**Figure 2.12a**).[211;212] Upon specific targeting of gold-antibody bioconjugates to an antigen, a red dot or band depicts a positive binding result, which enables evaluation with the naked eye (immunolabeling/sensing) (**Figure 2.12b**).[213;214]

Currently, multiple sensing applications based on this principle have been established for gold nanoparticle bioconjugates, such as ultrafast detection assays for deoxyribonucleic acid (DNA) hybridization,[216;217;212] locked nucleic acid (LNA) triplex formation,[218] en-

zyme-linked immunosorbent assay (ELISA) for protein testing,[219-221] sugar sensing[222;20] and cell sensing.[223-225] Researches have also found applications that can be used in daily life around the world. Examples of this are ready-to-use test strips that function based on the immunoflow method for e.g. pregnancy[226] ('*Clearblue*' — SPD Swiss Precision Diagnostics GmbH, Switzerland), cancer (ScheBo Biotech AG, Germany), myocardial infarct[227] (Novamed Israel) (**Figure 2.12b**) or drug screening[228] ('*DrugCheck*' — Express Diagostics Int'l Inc., USA).

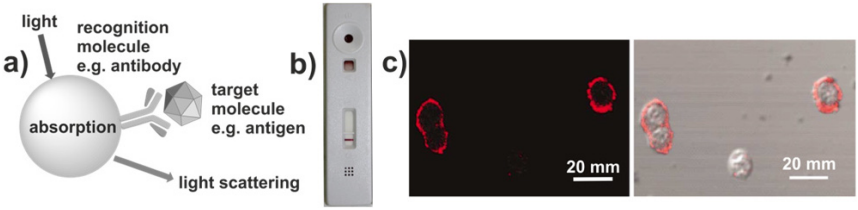

Figure 2.12. **Sensing of target molecules and imaging of cells with AuNP bioconjugates. a)** Scheme of sensing process. **b)** Commercial test stripe for the sensing of myocardial infarcts, based on immunoflow principle. © 2015 Novamed Israel. **c)** Specific detection of cancer cells by light scattering of AuNP bioconjugates (red coloration) which coupled to the cell membrane by cancer cell-specific antibodies. Reprinted with permission from Sokolov et al., copyright 2003 by SAGE Publications Ltd.[215]

The specific immunolabeling may further provide an accumulation of AuNPs in a distinct area of interest, e.g. on target cells via cell-specific membrane markers (cluster of differentiation (CD) molecules). With this accumulation, adequate contrast can be provided for the optical imaging of tissue and cells via the light scattering detection of AuNPs both *in vitro* and *in vivo*.[215;229-233] In this context, Sokolov et al. visualized cancer cells that were over-expressing the epidermal growth factor receptor (EGFR) by CLSM after incubation of cells with anti-EGFR antibody-coupled AuNPs (**Figure 2.12c**).[215]
In addition, the specifically targeted and AuNP-accumulated cells may be separated from a mixture by sorting methods such as flow cytometry. Either the light scattering property of AuNPs is used for contrast differentiation of the cells [234;235] or fluorophore-functionalized AuNP bioconjugates are applied for fluorescence-activated cell sorting (FACS).[236;237]

Photothermal cancer therapy

A common medical treatment for cancer is the local temperature increase of malignant tissue by hyperthermia therapy.[238] The restricted overheating in the range of 40 to 44 °C increases the blood flow and thereby enhances the efficiency of chemotherapy. Moreover, the heat is confined to the tumor because dissipation into the surrounding tissue cannot be established due to a simple and compact vascularization. This causes nutrient depletion, which leads to a reduced metabolism and reparability. That in turn, might induce a cellular dieback.[238] If very high temperatures > 50 °C are applied, an ablative destruction

of tumor cells could be achieved; however this method involves the insertion of a cannula directly into the tumor.[239]

There are several approaches to cancer hyperthermia, such as microwave, radiowave or ultrasound treatment, the adoption of magnetic nanoparticles and the laser-induced thermotherapy. Among those approaches, the number of publications on hyperthermia therapy with magnetic nanoparticles has increased significantly in the past decades.[240-243] The method requires the oscillation of the particles in an alternating electric field with local heat development.[244] Thus, tumor cells that contain the magnetic nanoparticles are thermally destroyed.

However recently, biofunctionalized gold nanoparticles have become an area of interest and several workgroups have utilized them with heat therapy for cancer.[245-247;5;96]

This approach is based on the plasmon-coupled heat release into the environment using light irradiation of the gold nanoparticles and is also known as plasmonic photodynamic therapy (PPTT).[249] Due to heating zone development and the explosive evaporation of water around the particles, emerging bubbles cause the formation of irreversible pores in the tumor cell membrane (**Figure 2.13a**).

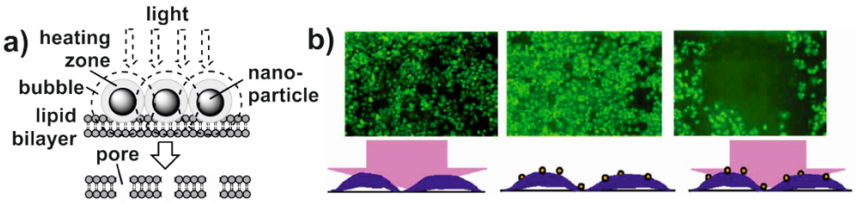

Figure 2.13. Photothermal effect of AuNP bioconjugates on malignant cells. a) Scheme of membrane pore formation principle upon light irradiation of membrane-attached gold nanoparticle bioconjugates. **b)** Photographies (upper row) and schematic illustration (lower row) of cancer cell destruction by photothermal treatment. Green coloration = cancer cells, yellow dots = AuNP bioconjugates. Reprinted with permission from Loo et al., copyright 2004 by SAGE Publishing Ltd.[248]

With this photothermal effect, malignant tissue is destroyed locally when AuNPs that are coated with tumor-specific marker bind to the cancer cells. This was shown in a successful study by Loo et al. (**Figure 2.13b**).[248] When attempting to achieve a high tissue penetration and less off-target absorption, near-infrared lasers are often applied.[249]

Moreover, the transient permeability of the cell membrane after laser heating enables the cellular uptake of extracellular molecules, which may support cancer treatment.[250;251]

Delivery and switchable release of effector molecules

To achieve optimal effectivity of pharmaceutics and to perform gene silencing using short-interfering RNA (siRNA), large numbers of the effective molecules must be deliv-

ered to a defined intracellular area of interest that contains specific CD-bearing cells such as the nucleus, while an overall *in vivo* distribution is hindered.
A variety of methods for the intracellular delivery of effector molecules has been developed for this intent, including the adoption of viral vectors and the transient pore formation that was mentioned previously.[250;252;253] However, most of these methods lack specificity and suffer from insufficient delivery efficiency and low throughput.

Regarding solid tumors, the passively-targeted accumulation of gold nanoparticles at their proliferating sites with the enhanced permeation and retention (EPR) effect has already been explained.[254;255] Furthermore, AuNP functionalization with specific antibodies allows the active targeting of CD-bearing cells, which was also discussed previously. Thus, the simultaneous conjugation of effector molecules and antibodies to AuNPs could enable a directed delivery.

In the last decade, gold nanoparticles have actually been determined to be efficient transport vehicles for the intracellular delivery of effector molecules such as under-expressed substrates,[256] oligonucleotides and siRNA[257] or drugs.[258] In addition, the receptor-specific delivery using bivalent gold nanoparticle bioconjugates functionalized with a pharmaceutic and an aptamer was also presented.[259]

However, to obtain maximal effectivity it may be necessary for the cargo to be separated from the AuNP transport vehicles once the area of interest is reached, especially if gene modifications within the condensed nucleus are the target.
For this intent, the delivery process may be combined with the switchable, light-induced release of cargo at the place of destination by separating a photocleavable linker or by melting gold nanoparticles via irradiation (**Figure 2.14a**).[210;260]

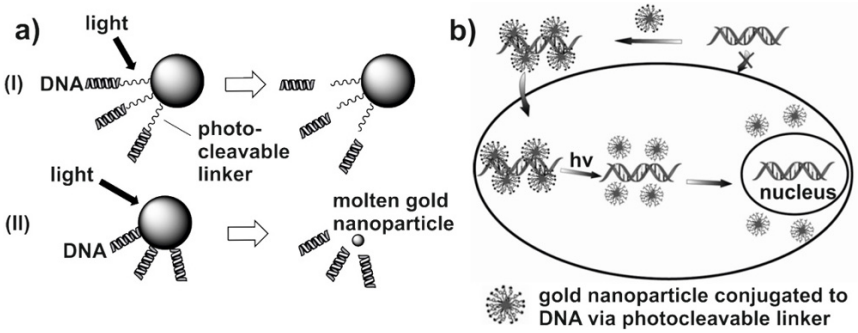

Figure 2.14. Directed delivery of effector molecules using AuNPs as transport vehicles. a) Scheme of light-induced ligand separation from AuNP bioconjugates via photo-cleavage of a linker (**I**) or by particle melting (**II**). **b)** Non-invasive delivery of DNA into the cell nucleus by AuNP bioconjugates. Adapted from Han et al.., copyright 2007 by Springer Science + Business Media.[210]

In this context, Han et al. presented the non-invasive delivery of DNA into cell nuclei by ensuring that gold nanoparticles were safely transported through the cell membrane and by using a photocleavable linker on the AuNPs for light-induced separation of the ligand molecules (**Figure 2.14b**).[261] Furthermore, Poon et al. showed the controlled denaturing of Au-S bonds due to photothermal dehybridization in response to pulsed laser irradiation.[262]

Actually, a selective release of cargo from gold nanorods has previously been demonstrated by Wijaya et al.[260] In their experiments, nanorods with different aspect ratios were selectively melted by irradiation with adequate laser wavelengths, which led to a controlled delivery of the DNA ligands.[260]

In summary, AuNP bioconjugates are widely used in biomedical and reproductive research and their application prospects are growing rapidly. The combination of selective targeting/delivery, therapy and sensing/diagnosis has established a new field of research termed *theranostics* which are smoothing the way for the personalized medicine of the future.[263] However, in order to achieve the proper combination of specific functionalities, the properties of gold nanoparticles must be modified for each individual application and thereby specific design criteria need to be considered.

2.6. Design criteria of gold nanoparticles

How to achieve biological functionality for specific demands

Discussing gold nanoparticles, one may classify their properties as being intrinsic or caused by additional functionalization. Particles' intrinsic properties cover primary particle size, shape and charge while additional properties may be configured via conjugation with functional molecules. Due to a high affinity of sulphur to gold surfaces and a strong thiol-gold bonding, thiolated biomolecules attach nearly covalently to the particles, resulting in stable gold conjugates. Since specifications of AuNP bioconjugates need to be adjusted to meet the individual demands of biomedical requests, 6 regulative design criteria may be defined. Biocompatibility **(I)** of conjugates is the main facet for applications regarding biomedical science, but also aspects covering selective receptor coupling **(II)**, cellular penetration **(III)**, effect initiation **(IV)**, imaging **(V)** and *in vivo* resistance **(VI)** must be matched with regard to the individual objective (**Figure 2.15a**).

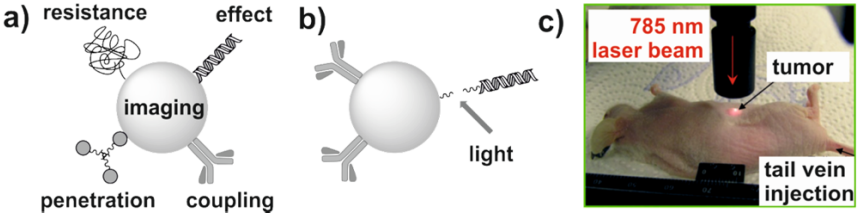

Figure 2.15. Customized AuNP design and effectivity. a) Scheme of an individual particle design with four specific attributes. **b)** Scheme of effect initiation with a potential stimulus, such as e.g. light irradiation. **c)** Tumor detection and treatment by laser excitation of accumulated AuNP bioconjugates *in vivo*. Adapted with permission from Qian et al., copyright 2008 by the Nature Publishing Group.[232]

For instance, the *in vitro* detection of tumor cells requires biocompatibility, nanoparticle coupling to a tumor specific receptor and bio-imaging of particles, while the photothermal therapy of cancer depends on additional *in vivo* resistance and cellular penetration. In this context, the customized design of gold nanoparticle bioconjugates is not trivial and should be carefully considered, with special regard to the multivalent functionalization of particles.[264] Thus, with controlled coupling of distinct ligands to a single gold nanoparticle, all three required design criteria for tumor cell detection can be matched with a single multivalent nanobioconjugate.

In addition to a customized design, a second aspect regarding the functionality of gold nanoparticle bioconjugates involves the utilization of switchable and mainly light-induced stimuli (**Figure 2.15b**). With external irradiation of intracellular particles, effects such as the aforementioned ligand separation[261] or particle aggregation[265] are triggered. Particle aggregation may be necessary to induce a higher extinction cross section of nanoparticles for detection or therapeutic issues within the NIR therapeutic window at the accumulation area (**Figure 2.15c**).

Thus, the tunable structure-function relationship of gold nanoparticle bioconjugates as well as their strong ligand binding and ability to carry diverse functional classes simultaneously, characterize them as perfect candidates for biomedical research applications.
To review the design criteria of gold nanoparticles, effect initiation (**IV**) may be induced by stimulating the plasmon-coupling for photothermal therapy or with the conjugation with effector molecules. The conjugates are mainly applied for the delivery of pharmaceutical drugs to inflammation areas or cancer cells. These aim on a local, stimuli-induced activation of ligands at the area of interest in order to avoid full-body medication.[259;258;266] Whereas, a second issue implies the transport of regulative moieties like oligonucleotides,[218;267;39] siRNA[257] or glutathione[256] for therapeutic applications on the gene and protein levels. With regard to receptor coupling (**II**), recognition molecules such as aptamers[268;269] or antibodies[270;36;271;221] are generally attached to gold nanoparticles to

achieve specific binding of the nanoconjugates to targeted cells or intracellular fragments. With regard to *in vivo* resistance (**VI**), masking molecules such as poly(ethylene) glycol[118] or albumin[272] are often applied to camouflage nanoparticles from immune system recognition and inflammation reaction.
However, these described design criteria mainly depend on conjugated moiety, whereas imaging (**V**), penetration (**III**) and biocompatibility (**I**) criteria of gold nanoparticle conjugates are more often connected with the particles' intrinsic characteristics and will not be discussed in detail within this thesis.

In summary, the appropriate design of nanobioconjugates is crucial for their biological functionality and highly dependent on their task and field of application. Six regulative criteria are defined and should be adjusted carefully for each bioconjugate, with respect to the biomedical request.

2.7. Fabrication of gold nanoparticles and AuNP bioconjugates

2.7.1. Conventional fabrication methods

Nanoparticles are generally defined as spheres between 1 and 100 nm in diameter.[273] Their common states of appearance are solid powders, gaseous aerosols and colloidal dispersions in water or organic solvents. Among those, colloids are often preferred for research due to their safe and stable handling form, which will reduce the risk of particle inhalation.
Focusing on the fabrication of gold nanoparticles, a multiplicity of fabrication methods have been established in the last decades, which are typically grouped into chemical (bottom-up, precursor-based) and mechanical/physical (top-down, precursor-free) synthesis approaches. In addition, there are also some exotic generation techniques e.g. the synthesis in plants and yeast.[274;275]

The mechanical top-down generation of AuNPs may be performed by grinding gold powder to a nanoscaled dimension[276] using e.g. a planetary ball mill. Although a high volume may be processed at once, the drawbacks of this approach are a high polydispersity of nanoparticle sizes, a limitation of minimum size, extremely long grinding times of days to weeks and contaminations that arise by abrasion of grinding gears. In general, the grinding method is more common for the size-reduction of e.g. carbonate nanoparticles than for AuNPs.[277]
Thermolysis has been used as a top-down physical method to produce alkyl-group passivated AuNPs.[278;279] However, heat-treated AuNPs often form 2D superlattices which may limit their biological application.[280]

The most economic method for AuNP generation is the chemical bottom-up synthesis, which can be carried out in a solid, liquid or gaseous state, implying the configuration of structures based on an atomic level. In addition to the chemical fabrication of AuNPs using microemulsions,[281] (copolymer) micelles[282] and seed growth,[283] the most common chemical technique is the wet-chemistry chemical reduction method (CRM), involving the nucleation, growth and agglomeration of atoms into nanoclusters. CRM was originally discussed in 1857 by Michael Faraday, who prepared gold hydrosols by reducing an aqueous solution of chloroaurate with phosphorus dissolved in carbon disulfide.[60] During the next century, various standard protocols were developed.[284;37;38;285;286] In the general CRM principle, Au^{3+} ions of a gold salt such as chlorauric acid ($HAuCl_4$) are reduced with reduction agents such as sodium borohydride[37] or sodium citrate[38] to zero-valent gold atoms (nucleation) (**Figure 2.16** and **Figure 2.17a**).

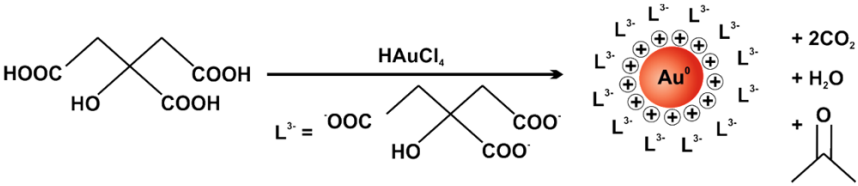

Figure 2.16. Reaction scheme of the Turkevich method for citrate-stabilized AuNP fabrication. Adapted from M. Noyong, copyright 2005 by Michael Noyong, dissertation.[287]

These gold atoms collide with other atoms or ions in the solution and grow into stable *seed nuclei*. As more and more of these nuclei form, the solution becomes supersaturated and the gold begins to precipitate in the form of (sub)nanometer particles. Further growth and agglomeration of the seed nuclei is then controlled with stabilizing agents such as sodium citrate or thiol ligands that protect the particle surface and allow for a precise and monodisperse nanoparticle size control (**Figure 2.17a**).

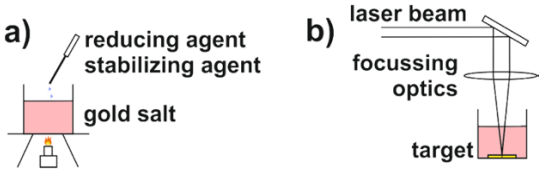

Figure 2.17. Chemical and physical synthesis approach for the generation of AuNPs. a) Scheme of chemical reduction method. **b)** Scheme of pulsed laser ablation in liquids process.

However, the biocompatibility of stabilizers is often restricted, e.g. as shown by Massich et al. that citrate may cause cell death by apoptosis.[121]

The functionalization of CRM-fabricated gold nanoparticles with biological active moieties is commonly facilitated by a successive substitution of the stabilizing agent with the

functional ligand molecules in a so-called *thiol-mediated ligand-exchange reaction*.[288-290] Unfortunately this procedure is known to be inefficient, due to a significantly high ligand excess and low degree of functionalization of the fabricated AuNP bioconjugates.[291]

In summary, the bottom-up chemical synthesis of AuNPs is the most economic fabrication route compared to conventional top-down or biological synthesis approaches. However, although a controlled monodisperse colloid may be gained by CRM, the AuNPs bear stabilizers on their surface which may induce cytotoxic effects and which limit the functionalization efficiency of exchange reaction. Thus, a method to fabricate stabilizer-free AuNPs is required.

2.7.2. Pulsed laser ablation in liquids

The physical AuNP synthesis approach with pulsed laser ablation in liquids (PLAL) has become a reliable alternative to the conventional CRMs. The principle refers to the removal as well as the nucleation and growth of nanoparticulate material with a complex physico-chemical processes during laser irradiation of a solvent-immersed target.[40;292] Thus, it cannot be clearly assigned to either the top-down or the bottom-up approaches.

The basic experimental set-up was pioneered by Patil et al. in 1987, when they ablated an iron target in water to produce an iron oxide coating on a surface.[293] Six years later, Henglein applied that method for the fabrication of colloidal gold nanoparticles.[294] To date, many research groups have adopted this technique for AuNP generation (**Table SI 14**)) using lasers with femtosecond (fs), picosecond (ps) and nanosecond (ns) pulses at visible or near infrared wavelength. Among them, infrared wavelengths are preferred, since most solvents are transparent in this spectral regime and spherical metal nanoparticles usually do not feature extinction in the NIR regime.

The PLAL process offers specific advantages compared to conventional fabrication methods:
(I) The precursor-free environment allows the fabrication of highly pure (100 %) gold nanoparticles with surfaces free from any contaminations and without the requirement for purification in water and organic liquids. A selective overview of recent publications is found in **Table SI 14**. Because no chemicals are involved and no waste is produced, PLAL may be termed as a *clean* fabrication technology.
(II) There is no requirement for stabilizing additives because the PLAL-generated nanoparticles are usually charged, which results in strong particle repulsion and colloidal stability. Moreover, charge delivery by micromolar anions improves stability und monodispersity of fabricated nanoparticles.[295]

(III) The fabricated particles provide a high degree of occupational safety because they cannot cross the liquid-gaseous interface into the air. Thus, they are not inhalable and do not cause health risks compared to the ablation in air.[296]
(IV) The process is highly variable because there are only few limitations with the materials to be ablated. The aforementioned nanoparticle fabrication of metals,[297;298;292] alloys[299;300] and ceramics[301;302] adds to the variability of the process. Likewise, various liquids such as water, organic solvents and saline media that are transparent to the laser wavelength may be adopted, which leads to a significant number of possible material-solvent combinations.[303;41]
(V) No complex experimental arrangements (e.g. vacuum chambers and nanoparticle collectors) are required for PLAL. The general set-up (**Figure 2.17b**) consists of a pulsed laser system, a set of beam guidance and focusing optical components and a vessel that contains a solid material plate at the bottom, covered with a liquid layer of ablation medium. Furthermore, the process may be accomplished on the time-scale of seconds to minutes, while production up to milligram scale for target ablation and up to the gram scale for wire ablation has already been achieved.[302;304]
(VI) The functionalization of laser-generated gold nanoparticles with biomolecules can easily be achieved with *in situ* or *ex situ* conjugation. *In situ* conjugation involves the direct addition of the functionalization agent to the ablation medium prior to the laser process, thus enabling a simultaneous nanoparticle generation and functionalization in a single step.[39] In contrast, during *ex situ* conjugation, the functionalization agent is mixed with the particles in a second synthesis step.[305]

Despite these outstanding advantages, the current limitations of the PLAL process should not be neglected:
(I) Due to limitations of available ultrashort-pulsed laser systems regarding the combination of a high repetition rate with high pulse energy and ultrafast scanning speed, the yield of nanoparticles by target ablation is limited on the milligram scale and is on focus of current yield enhancement research.[301;302] Thus, commercial fabrication still lags behind the productivity of chemical synthesis.
(II) Monodisperse nanoparticle sizes in *MilliQ* water may not be gained by the PLAL process without the addition of stabilizers, biomolecules or inorganic salts. Instead of that, particle size distributions in the range from ten to one hundred nanometers are developed in ultrapure liquids. Likewise, the particle shape is confined to spheres, while other shapes have only been produced in exceptional cases.[306]
(III) In order to control the phase and structure of PLAL-produced nanoparticles, it is strongly recommended, that the manufacturer has a deep understanding of the ablation mechanism and the physicochemical processes.

Ablation mechanism – laser-matter-interaction

Until recently, there has been a lack of knowledge concerning the physical and chemical processes during PLAL and the nanoparticle formation, that may take place with mechanisms such as nucleation or target-ejection of hot drops and solid fragments.[307] While the action of plasma processing is at least widely acknowledged,[308;309;292;310;40;303] the more complex reaction mechanisms between plasma species and the liquid media are not yet fully understood and different particle generation models have been proposed. Amendola et al.[311] classified six temporal stages of ablation process (**Figure 2.18**):

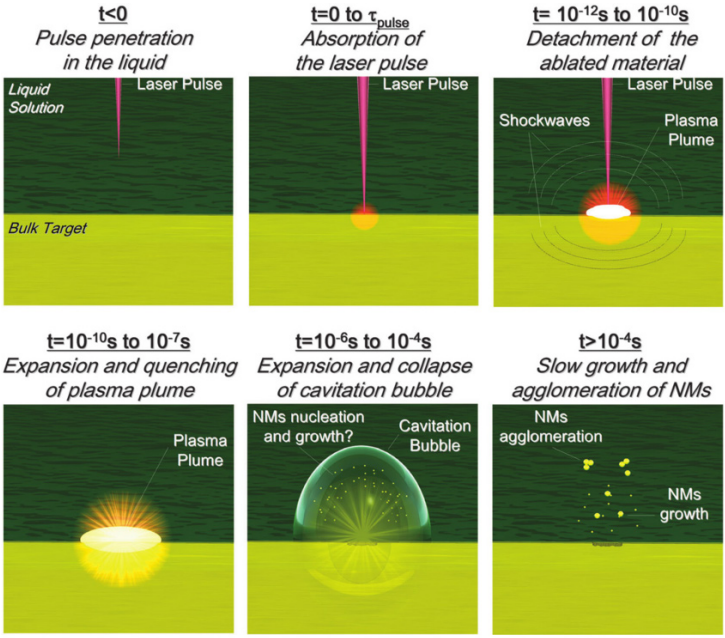

Figure 2.18. Illustration of PLAL process. Presented on the example of ns-PLAL with fluence above the ablation threshold and hypothesized time ranges. NM = nanomaterials. Reprinted with permission from Amendola et al., copyright 2013 by the Royal Society of Chemistry.[311]

(I) Pulse penetration in the liquid

In an ideal scenario, the liquid solution should be transparent at the adopted laser wavelength to enable delivery of laser energy to the target without solvent absorption. To avoid liquid breakdown effects when working with pulses of picoseconds or longer durations, defocused conditions should be followed. Whereas, to avoid nonlinear optical effects like self-focusing when working with femtosecond pulse durations, the liquid layer thickness must be reduced to maintain the defocusing conditions. In all cases, to avoid

nonlinear optical effects like multiphoton absorptions from the liquid, the critical fluence threshold (F_{th}) must not be exceeded.[312;311]

(II) Absorption of the laser pulse

Using nanosecond or long picosecond laser pulses for ablation, photonic energy of the laser beam is coupled to the electrons of the bulk material, which start to oscillate rapidly. The interplay of fast moving electrons with the stationary atoms through electron-phonon interactions transfers the energy and cools the electrons. This transfer causes energy vibrations in the lattice and consequently, phonon-phonon interactions that create lattice waves in the target material and enable thermal material removal by melting or thermal vaporization.[313;311]

On the contrary, laser pulses with high fluences and pulse durations shorter than the time needed to couple the electronic energy to the lattice (femtosecond or short picosecond) cannot initiate electron-phonon and phonon-phonon interactions in the target material. For this reason, there is no or very little thermal damage to the target surface.[313;311]

(III) Detachment of the ablated material

Using nanosecond or long picosecond pulses, the propagation of shockwaves in the material damages a thin layer of the target surface beyond the focal spot.[313;311] If laser irradiance is above the melting threshold of the target but below its vaporization threshold, surface melting of the target and formation of liquid droplets of target material occurs. These liquid droplets can be termed *molten globules*. On the contrary, if laser irradiance is higher than the vaporization threshold, vapors are generated from the target material at the solid-liquid interface. The front part of the laser pulse ionizes this material vapor to create hot laser plasma called *plume*. The plume absorbs and screens the last part of the laser pulse from the bulk material surface (plasma shielding). Thus, a comparatively smaller amount of energy is transferred to the target surface for materials removal.[313;311]

Conversely, for femtosecond or short picosecond pulses, the comparatively higher irradiance than the vaporization threshold causes the delivery of the maximum part of laser energy in a very short duration and the homogeneous, non-thermal, explosive ablation and fragmentation of material on the target surface. Furthermore, the laser pulse terminates before the energy is completely redistributed in the solid and no laser-plasma interaction will occur.[313;311]

(IV) Expansion and quenching of plasma plume

The plasma plume forms at or near the surface and propagates back up the laser beam. It is an expanding, thermodynamic state of high temperature, high pressure and high density.[314] During expansion, the plasma plume cools down and releases energy (heat) into the liquid solution. Thus, the laser-induced plasma (which contains metastable species from the target material) heats the neighboring liquid layer at the plasma-liquid interface to

temperatures that are greater than the boiling temperature of the liquid. This occurs in conditions of standard pressure and thus generates plasma of liquid species, which may be termed *plasma-induced plasma*.[313] Because the plasma-induced plasma is sandwiched between the expanding plasma plume and the liquid, it develops strong pressure (confinement) which results in an explosive ejection of metastable atomic or ionic species from the laser-induced plasma into the plasma-induced plasma.[313;311]
These species are quickly cooled and become clustered into elemental, embryonic noble metal particles such as Ag, Au or Pt, or they react with species of the liquid media to form e.g. oxide, nitride or carbide compound nanostructures of active metals such as Fe, Si, and Al.

(V) Expansion and collapse of cavitation bubble
Due to high pressure differences after the rapid expansion of the laser plume and because there is an energy release into the surrounding liquid, the formation of a vapor bubble termed *cavitation bubble* is initiated at the laser-target interface.[313] The cavitation bubble expands in the liquid with supersonic velocity up to a millimeter radius, while its temperature and internal pressure drop to a value below the surrounding liquid. Thereafter, the bubble collapses on a time scale of hundreds of microseconds with the emission of another shockwave and accompanied by an energy release that is large enough to cause a secondary ablation of the material.[311;313]

(VI) Slow growth and agglomeration of NPs
After shockwave generation, the system reaches physical and chemical steady state again. At this stage, the NPs can experience a secondary growth due to a coalescence with ablated clusters that are still in the solution and because there is an attachment of free atoms and ions.[311;313] These collisions occur as result of the diffusive mobility and thermodynamic instability of the cluster states and the particle growth finishes on the milliseconds to seconds scale when all of the surrounding clusters and atoms are consumed.[315] This secondary growth and eventually the ejection of molten globules were assumed to be the main reasons for the broad size distribution of PLAL-generated NPs.[316;298] However, recently Ibrahimkutty et al. proposed that even in the cavitation bubble two different particle species may be distinguished (**Figure 2.19**).[317] These species are primary particles of approximately 8 to 10 nm average diameter and secondary particles with 45 nm average diameter that result from collisions of the primary particles.

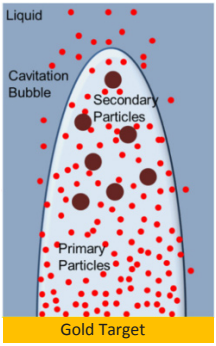

Figure 2.19. Illustration depicting two nanoparticle species found in the laser-induced cavitation bubble. Primary particles with a diameter of approximately 8 to 10 nm and secondary particles with an average diameter of 45 nm can be distinguished. Adapted with permission from Ibrahimkutty et al., copyright 2012 by AIP Publishing LLC.[317]

If the colloidal dispersion is not stable, agglomeration will begin, which results in particle precipitation on a timescale of minutes to days.[311;315] However, surfactants may be adopted to interact with the nanoparticles during condensation (or even within the cavitation bubble[295;318]) while preventing them from further coalescence and agglomeration through efficient stabilization and reduction of particle size distribution.[297;319]

2.8. Parameters affecting NP formation during PLAL

Points of consideration

During the PLAL process, there are several criteria that may affect the particle formation regarding the ablation medium, the presence of stabilizing agents as well as diverse laser and process parameters.

For instance, the particle size distribution (PSD) of AuNPs is generally broad after ablation in *Milli-Q* water (size distribution range: 5–140 nm[69]), compared to ablation in organic solvents[320;321] such as n-alkanes, dimethyl sulfoxide, acetonitrile and tetrahydrofuran, featuring size distribution that range on average from 2 to 10 nm. Moreover, AuNPs that were fabricated in nonpolar, organic solvents are often subject to aggregation on a time scale of days or weeks.[321]

The stability of AuNPs is a crucial aspect of their biofunctionality and to prevent agglomeration by van der Waal's attraction, the particles need to be stabilized by either electrostatic or steric repulsion.[322] In detail, three types of stabilization may be distinguished (**Figure 2.20**).

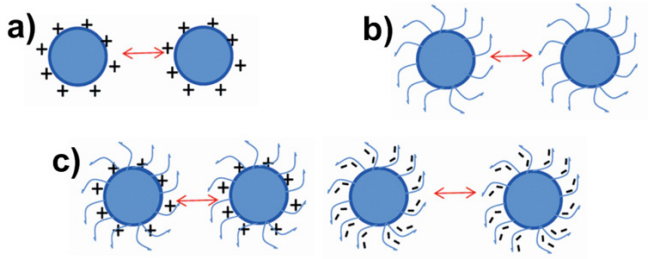

Figure 2.20. Three types of particle stabilization. a) Electrostatic stabilization. **b)** Steric stabilization. **c)** Electrosteric stabilization. Reprinted with permission from Liu et al., copyright 2014 by the Royal Society of Chemistry.[323]

If the NP surface is covered with charge carriers, such as ions, the equally charged particles will electrostatically repel each other in the solution. In 2004, Sylvestre et al. revealed with X-ray photoelectron spectroscopy, that the PLAL-fabricated AuNPs in *Milli-Q* water are not exclusively formed by metallic Au^0, but that they also contain Au^+ and Au^{3+} oxidation states that are mainly due to Au-O compounds.[324;325] They assumed those Au-O compounds are resulting from chemical reactions between the highly excited ejected Au atoms/ions or clusters and oxygen-containing species present in the laser-generated plasma or at the plasma/water interface. In addition, also carbonato complexes were detected ($Au\text{-}OCO_2^-$ and $Au\text{-}OCO_2H$), which are most likely resulting from the reaction of water-solved atmospheric CO_2 (as HCO_3^-) with the gold surface or after exposure of the dried sample to air.[324]

As a function of pH, either Au-OH or $Au\text{-}O^-$ is dominant; this yields a negatively charged surface with high zeta potential and electrostatic repulsion between the particles. This process is termed *electrostatic stability* (**Figure 2.20a**). Unfortunately, electrostatically stabilized particles are affected by high salt concentrations which screen the surface charges by reducing the electrical double layer thickness and result in particle agglomeration.[326;327]

In contrast to the AuNP fabrication in MilliQ water, the generation in organic solvents yields heterogeneous results. In polar solvents like acetone and alcohols, stable and non-aggregated AuNPs are obtained, due to adsorption of anions like enolates or alcoholates.[328] In contrast, in nonpolar solvents like n-hexane and toluene which are unable to give rise to anionic species, the resulting AuNPs are completely unstable and subject of aggregation.[328]

These particles need to be additionally stabilized with conjugation to ligands such as (charge-neutral) polymers or surfactants which prevent the close inter-particle contact with their long molecular chains. This effect is termed *steric stabilization* (**Figure 2.20b**). This effect was demonstrated by Compagnini et al. when they applied thiolated ligands for the steric stabilization of AuNPs in n-alkane, yielding long-term stable colloids without aggregation behavior.[329] Moreover, the structure of the nanoparticles was varied ac-

cording to the chain length of the sodium alkyl sulfate molecules and the shape could be turned from spherical to elongated through the appropriate molecular mass of the alkane molecules.[329] Different from electrostatic stabilization, the steric stabilized particles are not affected by high salt concentrations.
A combination of electrostatic and steric stabilization is termed *electrosteric stabilization* and defines ligand-stabilized AuNPs that bear and overall conjugate charge (**Figure 2.20c**). It does not matter thereby, whether the charge is located on the particle surface or on a polyelectrolyte ligand. This is the most common stabilization type for PLAL-fabricated AuNPs, yielding an optimized colloid stability and enhanced zeta potential. In this context, Muto et al. demonstrated the conversion of AuNP surface charge as a function of ligand concentration using a cationic surfactant and resulting in positive zeta potential values.[77]

Stabilization agents and other ligands have also been applied to limit the growth of nanoparticles during the nucleation process.[319;330-332] In this context, Mafuné et al. found that the particle size distribution of laser-generated gold nanoparticles shift to smaller sizes with the addition of sodium dodecyl sulphate (SDS).[319] The adjustment of particle size distribution by ligand addition was further reported by Besner et al., and Kabashin et al. who described a significant narrowing of size distribution as a function of increasing ligand concentration (**Figure 2.21a**).[330;332]
Moreover several groups reported that AuNP fabrication by PLAL in electrolytes with low salinity yield highly stabilized particles with small PSD.[324;318;295;333] The oxidized particle surface reacts efficiently with anionic species such as OH^-, Cl^- and Br^- in order to augment its net surface charge and to increase the electrostatic repulsion between particles.[318] The particle surface screening described earlier is not dominant in the applied micromolar concentration ranges and the anionic electrostatic stabilization is resulting from the Hofmeister effect[334] which defines stabilization and precipitation tendencies in proteins. Efficient size control was achieved with these means.[324;318;295;335]

Another possibility to narrow the particle size distribution of AuNPs is the re-irradiation of the colloid with a laser wavelength that is close to the SPR of gold (typically 532 nm laser). The size reduction can be a photothermal (ns, long ps pulses) and/or a photofragmentation (short ps, fs pulses) process, caused by multiphoton ionization. When there is a photothermal effect, the NP size is reduced as a consequence of their increased temperature up to the boiling point. Whereas, the reduction that occurs with photofragmentation has three steps; namely, the electron ejection form NP (leading to surface charging), the formation of a transient state in the NPs and the Coulomb explosion of surface atoms (fragmentation).[336]

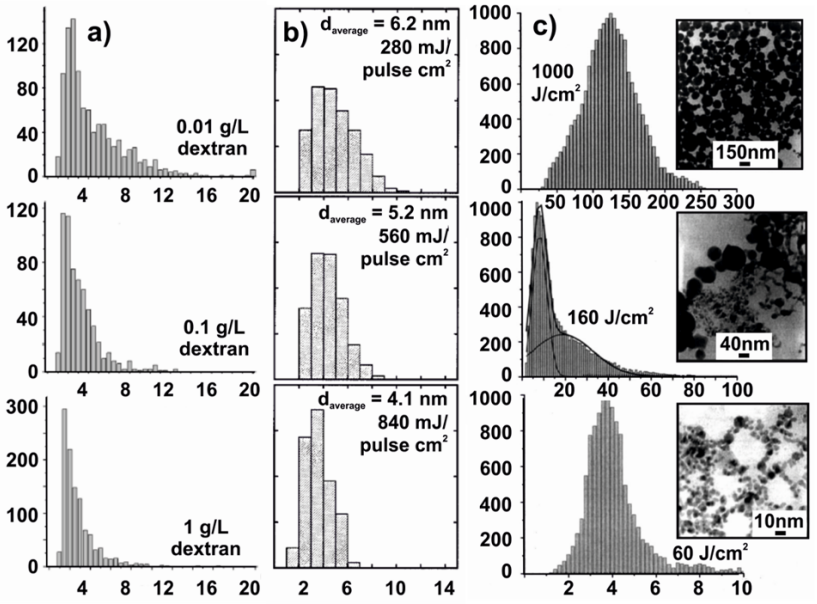

Figure 2.21. Examples on the modulation of PSD of AuNPs. a) PSD modulation as function of surfactant concentration. Adapted with permission from Besner et al., copyright 2009 by the American Chemical Society.[330] **b)** PSD modulation as function of re-irradiation fluence. Adapted with permission from Mafuné et al., copyright 2001 by the American Chemical Society.[316] **c)** PSD modulation as function of fabrication fluence during fs-PLAL with corresponding transmission electron micrographs.[298] Adapted with permission from Kabashin et al., copyright 2003 by AIP Publishing LLC.

The fragmentation efficiency is a function of laser fluence and Mafuné et al. presented that average 8 nm-sized AuNPs were fragmented to a 6.2, 5.2 and 4.1 nm average size for fluences of 280, 560 and 840 mJ pulse^{-1} cm^{-2}, respectively (**Figure 2.21b**).[316] Werner et al. further determined the threshold laser fluences of fragmentation to be 3.4 mJ cm^{-2} for fs laser induced fragmentation and found the process to be dominated by Coulomb explosion.[337]

The photofragmentation of *parent* nanoparticles causes gold atoms and small aggregates to be dispersed in solution, which can re-form smaller-sized *product* particles after condensation or which may be attracted by present NPs in the solution while growing them (coalescence).[338] The size, shape and phase of the nanoparticles might be changed during this process. Thereby, the coalescence rate increases with the concentration of small fragments until they are all consumed. Thus, a competition between fragmentation and coalescence takes place and the minimum particle diameter is only realized when the rate of fragmentation is equal to that of coalescence.[316]

Several studies have already been accomplished on a laser-induced photofragmentation effect on AuNPs after re-irradiation of the colloid with a focused or unfocused laser beam.[339-344;316;345;346;97;337]

Laser parameters such as pulse duration, wavelength, fluence and repetition rate may also influence the nanoparticle formation and should be considered carefully.
For instance, Riabinina et al found the ablation rate to be a function of pulse duration (40 fs–200 ps) with a maximum NP concentration at a pulse duration of 2 ps (using 5 mJ/pulse laser energy).[347]

Regarding wavelength dependency, Giorghetti et al. outlined an AuNP ablation with a 1064 nm wavelength that was more efficient than an ablation with a 532 nm wavelength. This was due to enhanced multiphoton absorption and photofragmentation of AuNPs using 532 nm wavelength.[342]
Kabashin et al. reported on the fluence-dependent particle size distribution of fs-PLAL generated AuNPs. While the thermal-free ablation occurs at low fluences (< 100 J cm^{-2}) and leads to very small and almost monodispersed colloids (3–10 nm), the plasma-induced ablation takes place at high fluences (< 100 J cm^{-2}) and results in much larger particle sizes and broader size distributions (5–70 nm; 25–250 nm) (**Figure 2.21c**).[298] Similar results were determined by Sobhan et al.[348] However, the low fluence regime is related to low production efficiency, which makes the higher fluence regime more attractive in practice. In this instance, the nanoparticle formation is more complex and may result in a two-component size distribution as reported by Sylvestre et al.[309]

Sobhan et al. and Ménendez-Manjón et al. discovered that a significant narrowing of NP size distribution occurred when the repetition rate was increased from 0.1 to 5 kHz.[349;344] Moreover, Sobhan et al. determined that narrowing was a function of irradiation time due to competition between ablation and photofragmentation.[349] Ménendez-Manjón also found that the narrowing was a function of liquid temperature that ranged from 283 to 353 K and which is directly related to a higher compressibility of water.[350] In another publication Ménendez-Manjón et al. showed that the flat-top (homogeneous) beam intensity profile yielded narrow, monomodal size distribution in the fluence range from 0.6 to 4.4 J cm^{-2}, while the Gaussian (inhomogeneous) beam intensity profile resulted in a bimodal size distribution. This was due to different thermalization pathways that formed during laser ablation.[351]

In summary, by tuning the fabrication parameters during the generation process, a flexible size adjustment of broad or narrowed size distributions with different distribution maxima can be provided for PLAL-generated AuNPs. In addition, the choice of ablation medium and the addition of stabilization agents will influence the formation of NPs and

modify their size, (shape) and stability. By these means, a precise modulation of intrinsic particle parameters is achieved.

2.9. Bioconjugation of AuNPs *in situ* during PLAL

Decoration and function

The term *bioconjugation* describes the linkage of biologically active molecules to nanoparticles by chemical or biological means, resulting in combinations of useful properties such as imaging and biological functionality.
Gold nanoparticles fabricated by CRM were conventionally bioconjugated using the thiol-mediated ligand exchange method as explained in **Chapter 2.7.1.** However, this procedure suffers from low surface coverages and it has difficulty equipping the AuNPs with more than one functional moiety due to affinity competitions between the different biomolecules to the gold surface.
Concerning the PLAL method, the linkage of NPs and biomolecules may occur after fabrication (*ex situ* bioconjugation). With simple mixing and a 24 h incubation of colloid and biomolecule solutions, the subsequent ligand coordination on the particle surface takes place either by thiol-gold bonding or electrostatic interactions (**Figure 2.22a**). In this manner, Salmaso et al. achieved the cellular internalization of laser-generated gold nanoparticles, conjugated to a thermosensitive polymer using the *ex situ* process.[117] However, the fabricated nanobioconjugates featured the typical broad PSD of laser-generated AuNPs, making them highly interesting for size screening experiments but inappropriate for size-limited applications
In another approach, Gamrad et al. fabricated size-quenched AuNPs (small PSD) with PLAL in micromolar salinity electrolyte (see **Chapter 2.8**) and conjugated the particles *ex situ* with CPPs in controlled ligand-per-particle ratios.[335] The presence of unbound ligands in the sample had to be considered, because no purification step was performed. However, the size quenching of nanoparticles during PLAL and the adoption of defined ligand-per-particle ratios, enabled the fabrication of highly controllable and reproducible nanobioconjugates.

Another approach was presented by Mafuné et al. in 2001.[319] They demonstrated that the addition of SDS surfactant to *Milli-Q* water prior to ablation leads to the formation of stable gold clusters with sizes that are smaller than those obtained in pure *Milli-Q* water, as a function of SDS concentration (see **Chapter 2.8**).[319]

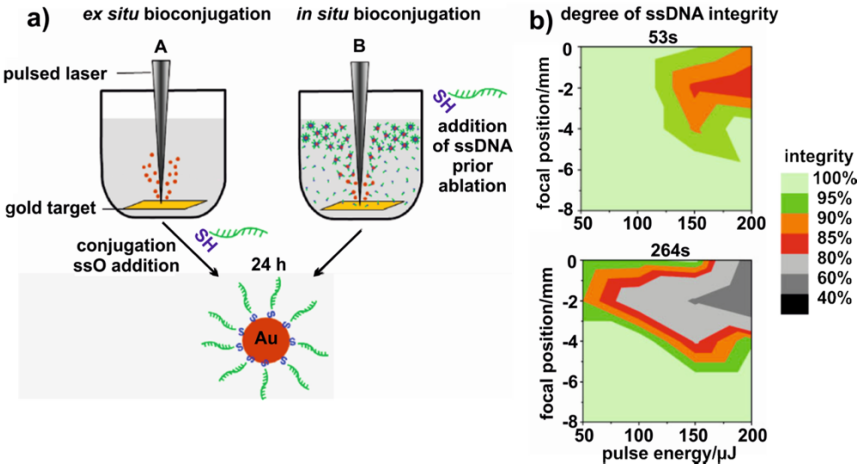

Figure 2.22. Bioconjugation methods of NPs and examples on the integrity of *in situ* bioconjugated AuNP bioconjugates. a) Scheme of *ex situ* bioconjugation (**A**) and *in situ* bioconjugation (**B**) methods with thiol-functionalized single-stranded DNA (ssDNA) that result in fabrication of functional AuNP bioconjugates. Reprinted with permission from Petersen et al., copyright 2009 by the American Chemical Society.[305] **b)** Integrity of ssDNA after 53 and 264 s laser ablation for different focal positions and pulse energies using a laser power of 0.5 W. Adapted with permission from Petersen et al., copyright 2009 by John Wiley and Sons.[39]

Obviously, the added surfactant competes with the particle growth processes during condensation (see **Chapter 2.7.2**) by decreasing the diffusion rate of small fragments and by covering the nanoparticles' surface while confining their size.[352] By this means, smaller NPs tend to be produced in a concentrated surfactant solution.[353] This observation is commonly termed *size quenching effect*[39] and because the coordination occurs during the fabrication process, the procedure was described as *in situ* bioconjugation (**Figure 2.22a**). The entire *in situ* process is highly sensitive to process parameters such as fluence, ablation time and focal position, since biomolecules are damaged easily by heat or physical degradation (**Figure 2.22b**).[39]

However, the AuNPs of Mafuné et al. were only stabilized by the SDS but did not feature any functionality due to conjugation. In 2009, the *in situ* conjugation of laser-generated AuNPs with biopolymers was demonstrated by Besner et al. for dextran-coated particles intended for biosensing of lectins.[330] In addition, the *in situ* conjugation of laser-generated AuNPs with functional biomolecules was enabled by Petersen et al. with single-stranded oligonucleotides.[39] Later, biological functionality proof of *in situ* functionalized gold-aptamer nanobioconjugates was demonstrated by Walter et al., by the efficient staining of prostate cancer tissue (**Figure 2.23a**).[269]

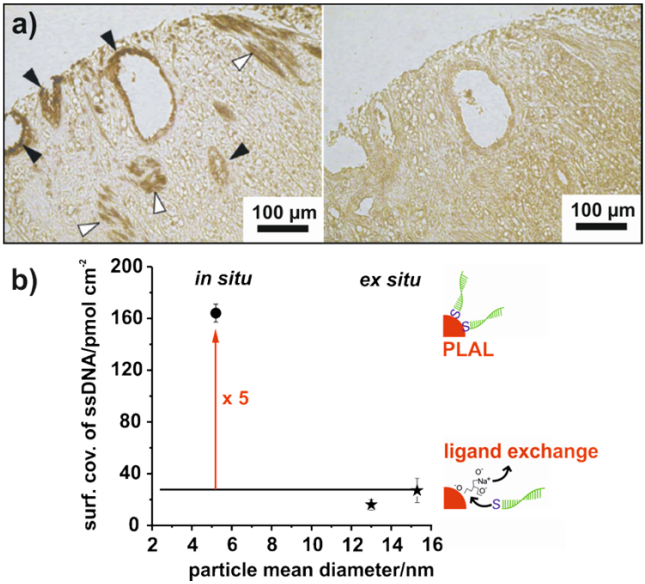

Figure 2.23. Functionality proof of *in situ* bioconjugated AuNP bioconjugates and example on obtained surface coverage values. a) Detection of PSMA in human prostate cancer tissue by immunohistochemical staining using anti-PSMA aptamer-gold nanobioconjugates (left image) and miniStrep aptamer-gold nanobioconjugates as negative control (right image). Black arrows = specific staining, white arrows = unspecific staining. Reprinted with permission from Walter et al., copyright 2010 by Walter et al., licensee BioMed Central Ltd.[269] **b)** Comparison of surface coverages (attached ligands per nanoparticle) obtained by *in situ* bioconjugation of laser-generated AuNPs (circle) and by *ex situ* ligand exchange on chemically synthesized AuNPs (stars). Adapted with permission from Petersen et al., copyright 2009 by the American Chemical Society.[305]

Since that time, research concerning the *in situ* bioconjugation of laser-generated AuNPs has gained more attention due to an enhanced biomedical demand for AuNP bioconjugates and because conjugation is easily accomplished in a single-step process.

Moreover, Petersen et al. determined that the *in situ* functionalization degree of laser-generated AuNPs with thiolated biomolecules is up to 5 times higher (**Figure 2.23b**) than for conventional *ex situ* conjugation of CRM-fabricated AuNPs in which the stabilization agents on the particle surface are exchanged in a thermodynamic manner with the ligands.[305] This enhanced cargo load is highly attractive for delivery applications (see **Chapter 2.5**). Thus, AuNP *in situ* functionalization with a wide range of biomolecules including oligonucleotides,[39;354;355] aptamers,[269] proteins,[356;357;40] antibodies[358] and cell-penetrating peptides[197] has been reported to date.

When looking at biological functionality, the thermal impact on the biomolecules during *in situ* conjugation must be fully understood. Takeda et al. determined that a significant lysozyme degradation took place as function of laser power and ablation time.[356] Addressing this issue, Petersen et al. reported a detailed study on biomolecule integrity and AuNP bioconjugate yield during the fs-pulsed laser ablation process. In this study, they assessed the ssDNA integrity as function of laser and process parameters such as focal position, pulse energy and ablation time (**Figure 2.22b**).[359] Using this model, optimal parameters can easily be characterized to ensure high biomolecule integrity and AuNP bioconjugate yield.

Alternatively, based on the approach of AuNP generation in liquid flow,[360] the *in situ* conjugation of AuNPs with fluorophore-labelled oligonucleotides was executed by Sajti et al. in a flow system.[354] Due to the flow-associated removal of molecules from the irradiation zone, they found a significant decrease in biomolecule degradation by a factor of 4 even at high pulse energies. These energies facilitate enhanced ablation efficiency and nanoparticle yield regarding economic cost-effectiveness[354] (**Figure 2.24a**).

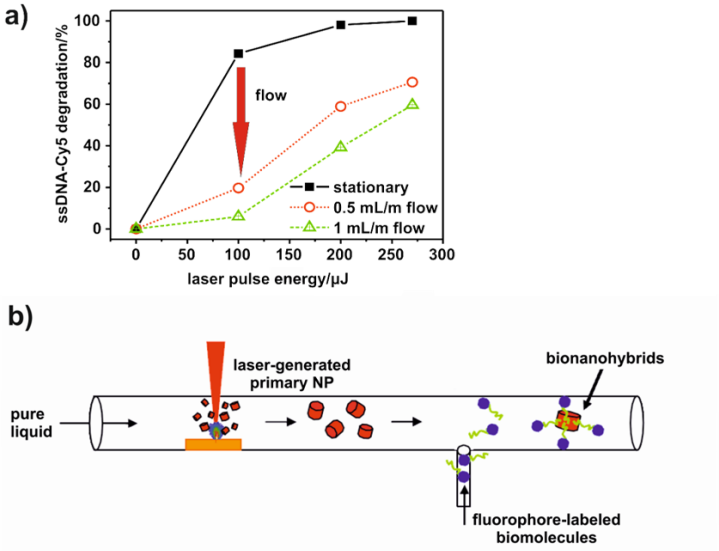

Figure 2.24. Bioconjugation of NPs in liquid flow and example on the biomolecule degradation during flow conjugation. a) The degree of biomolecule degradation in stationary liquid (black solid line) and liquid flow (0.5 mL/m flow: red dotted line, 1 mL/m flow: green dashed line) as function of laser pulse energy. Adapted with permission from Sajti et al., copyright 2010 by Springer Publishing Group.[354] **b)** Time-delayed, fast *ex situ* biomolecule conjugation to NPs in a liquid flow system. Adapted with permission from Sajti et al., copyright 2011 by the American Chemical Society.[361]

In a continuing study, biomolecule degradation was completely avoided with the delayed addition of ligands using a fast *ex situ* bioconjugation method in liquid flow (**Figure 2.24b**).[361]

In summary, PLAL-generated AuNPs may be functionalized with biomolecules during laser fabrication in a single-step, *in situ* process. The resulting AuNP bioconjugates feature higher surface coverage values than obtained by the chemical ligand exchange method. In addition, the AuNP bioconjugates show overall biological functionality if the biomolecule degradation is avoided by implementing adjusted PLAL parameters or adopting a liquid flow system.

2.10. Parameters affecting nanobioconjugate formation and function

Challenges and points of consideration

The bioconjugation of nanoparticles is a highly sensitive process, as various disfigurations of the nanobioconjugates may easily occur (**Figure 2.25a**).[362]
For instance, an incorrect ligand orientation can prevent the exposure of recognition epitopes and can therefore significantly reduce the biological functionality of the nanobioconjugates (**Figure 2.25a 1**). This is a main issue for the attachment of molecules which feature an active center such as antibodies, because their antigen-binding fraction (Fab) has to point outward from the NP surface to allow for the specific interaction and targeting of complementary ligand/analyte epitopes (**Figure 2.25b**, **Figure SI 1**).

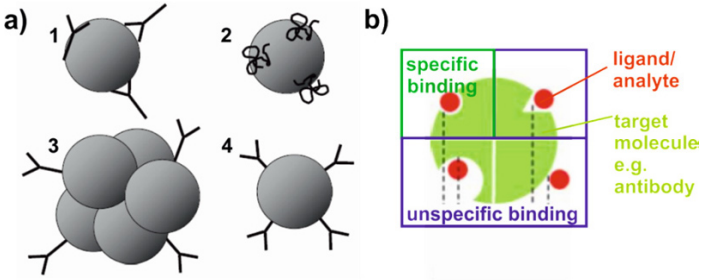

Figure 2.25. NP design requirements regarding ligand orientation and specificity. a) Different NP-antibody bioconjugate formations with **1** = wrong ligand orientation, **2** = ligand degradation, **3** = NP aggregation, **4** = ideal, functional NP bioconjugate. Reprinted with permission from Szymanski et al., copyright 2013 by Elsevier.[362] **b)** Scheme of specificity, illustrating different receptors binding options of a target molecules to a ligand/analyte. Adapted with permission from Yan et al., copyright 2012 by Macmillan Publishers Limited.[363]

The conventional adsorption of antibodies on AuNP surfaces with electrostatic interactions[229] generally yields a random ligand orientation that results in functional and non-functional molecules on the gold surface. High antibody concentrations are required for this approach and the attached ligands can easily be replaced by other molecules because of the weak electrostatic interactions. In a similar manner, also the EDC/NHS (1-Ethyl-3-(3-dimethylaminopropyl)carbodiimide/N-Hydroxysuccinimide) conjugation features the problem of orientation, since the terminal lysine amine groups used for attachment to a carboxyl group of a reaction partner are located at varying positions on the surface of the antibody.[364] Moreover, this method is generally used for nanoparticles that were chemically synthesized and equipped with a carboxyl function on their surface.
A covalent conjugation of antibodies can be achieved with different approaches such as the application of an orthopyridyl-disulfide-polyethylene(glycol)-N-hydroxysuccinimide (OPPS-PEG-NHS) linker or with an Avidin-Biotin system[365;366]. However, both linker systems are not specifically attaching to the non-targeting Fc region and thus they do not allow for a directed orientation of the antibodies on the AuNP surface.[366] Alternatively, the conjugation may be achieved with a heterobifunctional hydrazide-PEG-dithiol linker, which can specifically attach on the Fc portion of glycosylated antibodies while leaving the Fab portion unhindered.[270]

Another topic of disfiguration covers ligand degradation (e.g. by denaturating conditions) which can disable the biological functionality of the biomolecules (**Figure 2.25a 2**). Biomolecule degradation generally occurs with harsh environmental conditions such as inappropriate pH and high salt concentration in the solution or increased temperature that can denature the molecule irreversibly. However, disruption of the molecular structure (integrity reduction) as result of laser irradiation may also occur, especially if inappropriate laser parameters are used (see **Chapter 2.9**).
Finally, aggregation of nanoparticles can occur if the particles are insufficiently stabilized in solution or transferred from *MilliQ* water into high-concentrated salt solutions such as buffer media. This undesired particle aggregation can lead to *in vivo* issues like ineffective cellular uptake or renal clearing hindrance (**Figure 2.25a 3**; **Chapter 2.4**). Thus, ideal conjugation conditions are required to develop functional nanobioconjugates (**Figure 2.25a 4**).

Therefore, when considering PLAL and the *in situ* functionalization method, specific actions must be performed to avoid the formation of non-functional AuNP bioconjugates (**Figure 2.25a 1–3**).

- Correct ligand orientation is achieved by equipping the ligands with linkers which bind specifically to a molecule part at the opposing site of the active unit and which contain a thiol or a disulfide function for the covalent attachment to the gold surface.

- To avoid biomolecule degradation, either *ex situ* conjugation or the *in situ* conjugation has to be executed within a defined parameter window as presented in **Chapters 2.9** and **4.1.1.4.**
- NP aggregation is prevented by the PLAL process itself because partially oxidized and thus electrostatic stabilized particles are fabricated in *Milli-Q* water. However, if the conjugation must occur in non-polar solvents then the adoption of additional stabilizing agents might be required.

Another general issue that should always be considered is that due to local hydrophilic/hydrophobic patterns,[189] the nanoparticle surfaces will progressively and selectively adsorb biomolecules when they come into contact with complex biological fluids (e.g. cell culture media, blood), forming a biomolecule *corona*.[367;368] It is supposed, that the corona forms within 30 s of the nanoparticle's exposure to the culture medium and attaches to the particle surface irreversibly.[369] This corona is in many cases the part that interacts with biological systems and could affect or cover the functionality of former *in situ* attached ligands. Thus, it is recommended to have a stable (optimal: covalent) ligand attachment and complete coverage of the surface to reduce or control the corona formation. If this cannot be provided by the functional ligand itself (due to cost effectiveness) a PEGylation should be considered to cover the empty area on the particle surface. However, although surface modifications (such as PEGylation, or controlled presaturation e.g. with bovine serum albumin) block adsorptions spots and reduce the binding of additional biomolecules, some associations may still occur.[370;371]
According to these recommendations, *in situ* bioconjugation of AuNPs is generally performed with thiolized ligands and surface saturation is enabled by PEGylation with a thiolized PEG that is smaller than the functional ligand.

In the previous chapters, CLSM and optimal cellular uptake were discussed. Studies have shown that the mean size of primary nanoparticles must exceed a threshold limit, which according to several groups of researchers, appears to be 50 nm in diameter.[93;82] However, also smaller particles sizes may also be applied if controlled aggregation is achieved afterwards.[372;197] In addition, a positive particle charge strongly enhances particle internalization, while negative zeta potential is an intended property for colloidal stability, biocompatibility and low cytotoxic effects during particle uptake.[105]
These requirements are provided by PLAL-generated gold nanoparticles that feature a negative zeta potential and a partially positive particle charge due to the fabrication process. The particle distribution is tunable during the generation process or with subsequent photofragmentation and a positive net charge can be achieved with additional bio-functionalization, e.g. with cationic peptides.[335]

In addition to these basic design aspects, the customized design of AuNP bioconjugates may further be required to match specific biomedical applications. This customization generally covers the attachment of particular biomolecules, the defined surface coverage values or the multi-valent functionalization of particles with more than one functional ligand to match the combined medical demands and current research trends.[264]

In 2009, Petersen et al. highlighted the flexible adjustment of AuNP surface coverage with oligonucleotide molecules and found a saturation function with increasing biomolecule concentration.[305] In detail, using different nanoparticle to ligand ratios, the surface coverage of 5 nm laser-generated AuNPs with oligonucleotides was tunable from 10 pmol cm^{-2} up to 140 pmol cm^{-2}, which aligned with previous calculations of coverage data perfectly. Furthermore, the attractive issue of multi-valent functionalization may be addressed with different procedures including ablation and *in situ* bioconjugation in biomolecule mixtures or the *in situ* bioconjugation with a first ligand followed by subsequent *ex situ* conjugation with a second ligand.

In summary, the basic aspects of AuNP bioconjugate design including correct ligand orientation and surface masking should be considered prior to fabrication and are provided by *in situ* bioconjugation, if specific actions are followed.
Thus, with features such as a fabrication-related size-flexibility, good biocompatibility, imaging ability and conjugation potential with various functional biomolecules, PLAL-generated AuNP bioconjugates enable an individual and tunable design that can satisfy specific biomedical requirements and that may be used by biologists for a multitude of prospects.

http://www.springer.com/978-3-658-13514-0

Laser-Generated Functional Nanoparticle Bioconjugates
Design for Application in Biomedical Science and Reproductive Biology
Barchanski, A.
2016, XIII, 310 p. 134 illus., Softcover
ISBN: 978-3-658-13514-0